Superlattices and Microstructures, Vol. 25, No. 5/6, 1999
Article No. spmi.1999.0710
Available online at http://www.idealibrary.com on IDEAL

Quasiclassical Green's function approach to mesoscopic superconductivity

WOLFGANG BELZIG[†], FRANK K. WILHELM[†], CHRISTOPH BRUDER[†‡], GERD SCHÖN[†¶]

[†]*Institut für Theoretische Festkörperphysik, Universität Karlsruhe, D-76128 Karlsruhe, Germany*
[‡]*Departement Physik, Universität Basel, Klingelbergstrasse 82, CH-4056 Basel, Switzerland*

ANDREI D. ZAIKIN[§¶]

[§]*Forschungszentrum Karlsruhe GmbH, Institut für Nanotechnologie, D-76021 Karlsruhe, Germany*
[¶]*P.N. Lebedev Physics Institute, Leninskii prospect 53, 7924 MoscowRussia*

(Received 24 March 1999)

Recent experiments on mesoscopic normal metal/superconductor heterostructures resolve properties on length scales and at low temperatures such that the temperature is below the Thouless energy $k_B T \leq E_{Th}$. We describe the properties of these systems within the framework of quasiclassical many-body techniques. Diffusive and ballistic systems are covered, both in equilibrium and nonequilibrium situations. Thereby we demonstrate the common physical basis of various subtopics.

Key words: proximity effect, Andreev reflection, quasiclassical Green's functions.

1. Introduction

Quasiclassical techniques [1, 2] have become a widely used tool in the description of mesoscopic superconductivity. In comparison to early work which concentrated mostly on the regime near the superconducting transition temperature, recent work resolved much smaller length scales and covered lower temperatures. At temperatures below the Thouless energy, i.e. in dirty metals of size d for $k_B T \leq E_{Th} \sim \hbar D/d^2$, novel features have been observed. An important physical property is the proximity effect in a normal metal in contact with a superconductor. It is intimately related to the Andreev reflection [3], a process in which an electron incident from a normal metal tries to enter a superconductor. If its energy lies below the gap, it can do so only if it finds a partner electron with opposite momentum and spin to form a Cooper pair, leaving a retroreflected hole in the normal metal. In this process two charges are transferred into the superconductor. The reflection is phase coherent, since the electron and the reflected hole combine in a way consistent with the phase of the superconductor. The pair can maintain its phase information in the normal metal over a distance $\sim \hbar v_F/2E$, where $2E$ is the energy difference of the electron and hole. This space dependence, with diverging length scale at low energies, is responsible for several of the mesoscopic effects to be discussed below.

The proximity effect is characterized by the existence of superconducting correlations in the normal metal, expressed by a nonvanishing pair *amplitude*, $F \neq 0$. This is to be distinguished from the pair *potential* Δ, which in the absence of attractive interactions vanishes in the normal metal. Finally, the question whether

0749–6036/99/051251 + 38 $30.00/0

the normal metal shows a *gap* in the excitation spectrum is a more subtle issue. We will analyze below how the proximity effect reduces the tunneling density of states (DOS) at low energies, and, depending on the geometry, induces a gap or a pseudo-gap.

We will present here a unified view of both equilibrium and nonequilibrium properties of normal metal-superconductor proximity systems. The basis are the quasiclassical Green's functions, which will be reviewed in Section 2. Both the Matsubara and the Keldysh formalism are introduced. We discuss the clean and dirty limits, which allow systematic approximations. We finish the section with remarks on the boundary conditions and the strategies of solution. There exist several excellent introductions to this topic [4–6]. They have been written mostly with the goal of describing massive superconductors at temperatures near the transition temperature. Recent experimental work covered much lower temperatures and resolved properties on submicron length scales. We, therefore, present the theory and applications focusing on nano-structured systems at low temperatures.

In the following sections we will discuss several applications of the formalism and compare the results with recent experiments. In the equilibrium case (Section 3), we study the change in the local density of states (LDOS) in the vicinity of a normal metal - superconductor interface. It shows a strong suppression around the Fermi energy, leading to a minigap if the normal metal is finite in size [7, 8]. Our results agree with experiments performed by the Saclay group [9]. Next, we analyze the proximity-induced magnetic screening in a normal metal in contact with a superconductor. This allows us to describe the experiments of Mota and co-workers [10, 11] on the diamagnetic properties of normal/superconductor heterostructures. For a comparison, it is necessary to study the induced superconductivity in a material with intermediate strength of the impurity scattering. We found several new phenomena regarding the nonlocality of the current response in this regime [12]. Finally, we consider the supercurrent through a normal metal sandwiched between two superconductors, which allows us to interpret experimental results of Courtois *et al*. [13].

In Section 4, we study mesoscopic superconductors and heterostructures in nonequilibrium situations. The quasiparticle distribution function can be disturbed, e.g. by external applied gate voltages. Under mesoscopic conditions, it acquires a specific double-step form, which has been observed by the Saclay group [14]. This nonequilibrium form can be used, in a four-terminal geometry, to tune a supercurrent and, hence, to build a mesoscopic SNS transistor [15]. Moreover, the SNS junction can be switched by the gate voltages to become a π-junction. We can explain in this way recent experiments by the Groningen group [16–18]. A different SN heterostructure allows us to study the behavior of induced superconducting correlations on a dissipative current. In systems with transparent SN contacts, the dissipative conductance is enhanced, with a peculiar non-monotonic temperature and voltage dependence, usually referred to as 'reentrant' conductance [19, 20]. This means, at high temperatures the conductance grows with decreasing T since the proximity effect develops, it reaches a a maximum at $k_{\mathrm{B}}T \approx E_{\mathrm{Th}}$ where E_{Th} is the Thouless energy, and finally it drops back to the normal state value at $T = 0$. This behavior has been observed in experiments of the Grenoble group [21, 22]. In more complex, multiply-connected structures the proximity conductance can be modulated by an external magnetic flux. This modulation is dominated by states close to the Fermi surface, for which the spatial range of the proximity effect is large even at fairly high temperatures. This makes it possible to detect the influence of the proximity effect over distances much larger than the temperature-dependent coherence length [19, 22, 23]. In systems with tunneling barriers, the excess conductance competes with the conductance suppression at the tunneling interfaces governed by the opening of an induced gap. But even without tunneling barriers, the conductance may be reduced as a consequence of a four-terminal measurement in the thin film geometry [24–26].

The purpose of this paper is to demonstrate, by the use of quasiclassical many-body techniques, the common physical basis of several striking phenomena observed in recent experiments on mesoscopic superconductors and heterostructures. Of course, neither our presentation nor the bibliography can provide a complete review of the field. For a number of further applications of quasiclassical techniques we refer to articles in Refs [27–32] as well as the articles of Nazarov, Volkov, and Yip in this volume.

2. Quasiclassical formalism

2.1. Green's functions

Quantum field theoretical methods in terms of Green's functions are a powerful tool in all many-body problems (see e.g. [33–35]). Various systematic approximation methods and computation schemes have been formulated for them. In this section we will outline how they can be used, within a quasiclassical approximation to describe mesoscopic normal metal/superconductor proximity systems.

The starting point for all problems in superconductivity is the Green's function in Nambu space, which combines the particle and hole space [36]. Using the pseudo-spinors as a compact notation, $\hat{\Psi}^\dagger = (\Psi_\uparrow^\dagger, \Psi_\downarrow)$, we can express the time-ordered Green's function as

$$\hat{G} = -i\langle T\hat{\Psi}(1)\hat{\Psi}^\dagger(1')\rangle = \begin{pmatrix} G(1,1') & F(1,1') \\ F^\dagger(1,1') & G^\dagger(1,1') \end{pmatrix}. \tag{1}$$

The Green's function contains an 'anomalous' component, the pair amplitude $F = -i\langle T\Psi_\uparrow\Psi_\downarrow\rangle$, characteristic for superconducting systems. Using the BCS Hamiltonian, we can write the Gorkov equation of motion [33] for $\hat{G}$ as[†]

$$\begin{aligned} (\hat{G}_0^{-1} - \hat{\Delta} - \hat{\Sigma}_{\text{imp}})(1,2) \otimes \hat{G}(2,1') &= \delta(1,1') \\ \hat{G}(1,2) \otimes (\hat{G}_0^{-1} - \hat{\Delta} - \hat{\Sigma}_{\text{imp}})(2,1') &= \delta(1,1'). \end{aligned} \tag{2}$$

Here 1 and $1'$ represent sets of space and time coordinates and $\otimes$ includes a convolution over the coordinates. The free Green's function in Nambu space reads

$$\hat{G}_0^{-1}(1,1') = \delta(1-1')\left[i\hat{\tau}_3\frac{\partial}{\partial t_1} + \frac{1}{2m}\hat{\boldsymbol{\partial}}_{\boldsymbol{r}_1}^2 - e\phi(1) + \mu\right], \tag{3}$$

where $\hat{\boldsymbol{\partial}}_{\boldsymbol{r}} = \nabla_{\boldsymbol{r}} - ie\boldsymbol{A}(\boldsymbol{r})\hat{\tau}_3$ is the gauge-invariant spatial derivative. The part of the electron–phonon self-energy which is responsible for superconductivity defines the pair potential

$$\hat{\Delta}(1,1') = \delta(1,1')\begin{pmatrix} 0 & \Delta \\ \Delta^* & 0 \end{pmatrix} \text{ with } \Delta(1) = i\lambda \lim_{2\longrightarrow 1+} F(2,1). \tag{4}$$

Here λ is the strength of the attractive interaction. For a normal metal we have $\lambda = 0$ and hence $\Delta = 0$, but still the proximity effect manifests itself in a nonvanishing pair amplitude $F \neq 0$.

To simplify notations, we will from now on use center-of-mass coordinates in space and time and Fourier transform with respect to the relative coordinates.

Elastic impurity scattering will be included within the framework of the Born approximation. The impurity self-energy then reads

$$\hat{\Sigma}(|p|, R, E, t)_{\text{imp}} = \frac{\pi}{2\tau}\left\langle \int d\xi \hat{G}(\boldsymbol{p}, \boldsymbol{R}, E, t)\right\rangle_{\boldsymbol{p}_{\text{F}}}, \tag{5}$$

where τ is the elastic scattering time, $\xi = p^2/(2m) - \mu$ and $\langle \ldots \rangle_{p_{\text{F}}}$ denotes averaging over the Fermi surface. In contrast, we can neglect inelastic scattering, since we will study mesoscopic samples smaller than the inelastic length. Spin-flip scattering can be taken into account by an expression similar to (5), see [4–6].

The Gorkov equation can, in principle, be used to study mesoscopic proximity systems. However, these are genuine inhomogeneous systems. Hence, dealing with full double-coordinate Green's functions—while not impossible (see e.g. [37, 38])—may become very cumbersome, and typically one makes use of quasiclassical approximations in the course of the calculations anyhow. For a systematic and more efficient approach it is an advantage to perform this approximation already on the level of the equations of motion.

[†]Here and in the following we use units in which $\hbar = k_{\text{B}} = 1$.

2.2. The quasiclassical approximation

We will now formulate the equations of motion within the quasiclassical approximation. For simplicity, with the applications to be discussed in mind, we restrict ourselves to equilibrium and stationary nonequilibrium situations, although the quasiclassical approximation can be applied also to time-dependent problems, e.g. relaxation processes and collective modes [29].

The Green's function (1) oscillates as a function of the relative coordinate $|\boldsymbol{r} - \boldsymbol{r}'|$ on a scale of the Fermi wavelength λ_F. This is much shorter than the characteristic length scales in the typical problems in superconductivity, $\xi_0 = v_F/\Delta$ and $\xi_T = v_F/2\pi T$. Moreover, in those problems, it is important to study the phase of the *two-electron* wavefunction, which according to definition (1) depends on the center-of-mass coordinates. For these reasons it is possible, and sufficient for most applications, to integrate out the dependence on the relative coordinate. This has been recognized first by Eilenberger [1] and by Larkin and Ovchinikov [2]. We can add that the reduction is not allowed for another class of mesoscopic effects, e.g. weak localization and persistent currents, which are controlled by the phase coherence of the *single-electron* wavefunction, contained in the relative coordinates of (1). But these effects are usually much weaker than those related to superconductivity. On the other hand, the reduction is possible also for problems involving Andreev reflection, since the essential information is again contained in the *difference* of electron and hole wavevectors close to the Fermi surface.

2.2.1. Gradient expansion

When integrating over the difference variables, the convolution $\otimes$ in the Gorkov equation (2) (integration over internal variables) requires some care. It can be expressed, after the Fourier transformation, as a Taylor series

$$(A \otimes B)(\boldsymbol{p}, \boldsymbol{r}, E) = e^{\frac{i}{2}(\partial_{\boldsymbol{r}}^A \partial_{\boldsymbol{p}}^B - \partial_{\boldsymbol{p}}^A \partial_{\boldsymbol{r}}^B)} A(\boldsymbol{p}, \boldsymbol{r}, E) B(\boldsymbol{p}, \boldsymbol{r}, E), \tag{6}$$

where $\boldsymbol{r}$ refers to the center-of-mass coordinates. In the problems to be discussed we can neglect short-range oscillations, hence, we expand this expression up to linear order.

To proceed, we first subtract the Gorkov equation (2) from its conjugated form. We observe that the Green's functions and the self-energies are linear combinations of Pauli matrices *not* including the unit matrix. This simplifies the equation of motion to

$$[i\,\boldsymbol{p}\hat{\boldsymbol{\partial}}_{\boldsymbol{r}} + E\hat{\tau}_3 - i\hat{\Delta} - \hat{\Sigma}, \hat{G}] - \{\hat{\boldsymbol{\partial}}_{\boldsymbol{r}}(\hat{\Delta} + \hat{\Sigma} + e\phi + \mu), \nabla_p \hat{G}\} + \{\nabla_p \hat{\Sigma}, \hat{\boldsymbol{\partial}}_{\boldsymbol{r}} \hat{G}\} = 0. \tag{7}$$

This form is much simpler than the original. We note that it still accounts for particle-hole asymmetry, which is necessary, e.g. for the description of thermoelectric effects [39, 40].

2.2.2. Quasiclassical Green's functions

On the one hand, we want to ignore the information contained in the fast oscillations of the full Green's function $\hat{G}$ as a function of $|\boldsymbol{r}_1 - \boldsymbol{r}_2|$, which produces after Fourier transformation a pronounced peak at $|\boldsymbol{p}| = p_F$. On the other hand, we have to pay attention to the dependence on the transport direction, i.e. on the direction of the velocity, $\boldsymbol{v}_F$, at the Fermi surface. To make this explicit we write $\hat{G}(\xi, \boldsymbol{v}_F, r, E)$, where $\xi = \frac{p^2}{2m} - \mu$ depends on the magnitude of the momentum. The quasiclassical Green's function is then defined by

$$\hat{g}(\boldsymbol{r}, \boldsymbol{v}_F, E) \equiv \frac{i}{\pi} \fint d\xi\, \hat{G}(\xi, \boldsymbol{v}_F, \boldsymbol{r}, E), \tag{8}$$

where the integration contour has two parts covering both half planes, see [4] for details. From eqn (7) we obtain, from now on by setting $p = p_F$, the Eilenberger equation of motion for quasiclassical Green's

functions,

$$-[\boldsymbol{v}_{\mathrm{F}}\hat{\boldsymbol{\partial}}, \hat{g}(\boldsymbol{r}, \boldsymbol{v}_{\mathrm{F}}, E)] = \left[-iE\hat{\tau}_3 + \hat{\Delta} + \frac{1}{2\tau}\langle\hat{g}(\boldsymbol{r}, \boldsymbol{v}_{\mathrm{F}}, E)\rangle_{v_{\mathrm{F}}}, \hat{g}(\boldsymbol{r}, \boldsymbol{v}_{\mathrm{F}}, E)\right]. \tag{9}$$

The elements of $\hat{g}$ are

$$\hat{g} = \begin{pmatrix} g & f \\ f^\dagger & -g \end{pmatrix}, \tag{10}$$

which is still a linear combination of three Pauli matrices $\hat{\tau}_{1/2/3}$ with $f^\dagger$ being the time-reversed counterpart of f. This symmetry can be used for convenient parameterizations of the Eilenberger equation (see Section 2.6).

As the right-hand side of eqn (9) vanishes (in contrast to the Gorkov equation (2)), it only defines the Green's function up to a multiplicative constant. The constant can be fixed by the following argument: as $\hat{g}$ is a linear combination of the Pauli matrices, the square of the Green's function is proportional to the unit matrix $\hat{g}\hat{g} = c\hat{1}$. From eqn (9) we see that the proportionality constant c is space independent. If we now consider a system containing a sufficiently large superconductor, we can identify a region 'deep inside the superconductor'. Here $\hat{g}$ equals its bulk value, which can be calculated by performing the steps used in the quasiclassical approximation for the known solution [33] of the homogeneous Gorkov equation (2). This procedure yields $c = 1$, i.e. the Green's functions are normalized

$$\hat{g}\hat{g} = \hat{1}, \quad \text{i.e.} \quad g^2 + ff^\dagger = 1. \tag{11}$$

A more general, mathematical derivation of the normalization condition can be found in [39].

2.3. Kinetics and time ordering

From the knowledge of the retarded and advanced Green's functions alone, we can calculate energy-dependent quantities like the density of states

$$N(\boldsymbol{r}, E) = N_0 \mathrm{Re}\{\langle g^{\mathrm{R}}(\boldsymbol{r}, \boldsymbol{v}_{\mathrm{F}}, E)\rangle\}. \tag{12}$$

This, and similar expressions including the off-diagonal Green's function will be denoted in the following as *spectral quantities*. In thermal equilibrium these quantities also determine all properties of our system. Equivalently, the thermal Green's function maybe calculated in Matsubara imaginary-time technique. Then, the spectral quantities are found by analytic continuation.

In general, we need additional information on how the quasiparticle states are occupied, i.e. about distribution functions. To evaluate those under nonequilibrium conditions we will use the Keldysh technique. Both techniques are described in numerous references, so we will not rederive them but rather explain the basic idea and provide a practical guideline for using them in various situations.

2.3.1. Matsubara technique

The Matsubara Green's functions technique [41] has been developed to describe many-body systems in equilibrium at finite temperature [33, 34]. In thermal equilibrium, the eigenvalues of physical observables do not depend on (real) time. In order to calculate thermal expectation values, we trace over all states using the Boltzmann weight $\exp(-H/T)$, which can be viewed as analytic continuation of the time-evolution operator $\exp(iHt)$ to the imaginary direction $\tau = it$. It is sufficient to know this operator (and with it the Green's function) only in the interval $0 < \tau < 1/T$. By Fourier transformation and exploiting the Fermionic symmetry one sees that all the necessary information is contained in the Green's functions defined for a discrete set of energies $E = i\omega_n$, proportional to the Matsubara frequencies $\omega_n = (2n + 1)\pi T$ with integer values of n.

For those frequencies, in a bulk superconductor, the Green's functions read

$$g_\omega = \omega/\Omega,\ f_\omega = \Delta/\Omega \text{ with } \Omega = \sqrt{|\Delta^2| + \omega^2}. \tag{13}$$

This form will serve frequently in the following as a boundary condition. The Green's functions in imaginary times usually show no singular or oscillatory structure and behave rather smooth and monotonic. This, together with the fact that g_ω is real in the absence of fields or phase gradients, simplifies the numerical calculations in thermal equilibrium.

Expectation values of physical quantities can be expressed via Green's functions. To calculate thermal averages we rotate onto the imaginary time axis and perform the quasiclassical approximation. For instance, the result for the supercurrent density is

$$\boldsymbol{j}(\boldsymbol{r}) = -2ie\pi N_0 T \sum_\omega \mathrm{Tr}\langle \boldsymbol{v}_\mathrm{F} \hat{\tau}_3 \hat{g}_\omega(v_\mathrm{F}, r)\rangle. \tag{14}$$

In general, it depends nonlocally on the applied fields. Similarly, the self-consistency equation for the pair potential can be obtained from the corresponding expression (4) for Gorkov's Green's functions [33]. The integrations leading to the quasiclassical Green's function can be performed, and the self-consistency relation reads

$$\Delta = \lambda N_0 2\pi T \sum_\omega \langle f_\omega\rangle. \tag{15}$$

2.3.2. The Keldysh technique

The Keldysh Green's function technique [42] allows us to describe many-body systems outside equilibrium. Pedagogical reviews are given in articles [6] and books [43]. It has proven particularly useful in the description of nonequilibrium superconductors [4, 5, 29]. Again, we will not rederive the formalism, rather we summarize the concepts and some major results. We will later restrict ourselves to the dirty limit, although the Keldysh technique can be applied to ballistic systems as well [44].

By means of the Keldysh technique, it is possible to describe the real-time evolution of systems in nonequilibrium and at finite temperature. We assume that the system is initially, at $t = -\infty$, in a thermal equilibrium state. The time evolution of the system, for instance of its density matrix, is described by a forward and a backward propagator. Keldysh showed that this real-time evolution, as well as an evolution along the imaginary-time axis to account for thermal averaging, can be combined to a propagation along a single contour in the complex time plane, with a forward and backward branch running parallel to the real axis and a vertical part between $t = -\infty - i/T$ and $t = -\infty$ [42]. Green's functions are defined on this contour with time ordering along the Keldysh contour. Depending on whether the time arguments are on the forward or backward part, the Green's functions reduce to different analytic parts. For instance, the time-ordered Green's functions or the Kadanoff functions $G^{<(>)}$ can be obtained [35]. From those one obtains, by appropriate linear combinations, the retarded and advanced Green's functions, $\hat{G}^{\mathrm{R(A)}}$, as well as the Keldysh Green's function G^K. They are related by

$$\hat{G}^>(1,1') = i\langle \Psi^\dagger(1')\Psi(1)\rangle,\ \hat{G}^<(1,1') = -i\langle \Psi(1)\Psi^\dagger(1')\rangle, \tag{16}$$

and

$$\begin{aligned}
\hat{G}^\mathrm{R}(1,1') &= \theta(t_1 - t_1')[\hat{G}^<(1,1') - \hat{G}^>(1,1')] \\
\hat{G}^\mathrm{A}(1,1') &= -\theta(t_1' - t_1)[\hat{G}^<(1,1') - \hat{G}^>(1,1')] \\
\hat{G}^\mathrm{K}(1,1') &= \hat{G}^>(1,1') + \hat{G}^<(1,1').
\end{aligned} \tag{17}$$

To compact notations, these Green's functions can be written in matrix form in 'Keldysh space',

$$\check{G} = \begin{pmatrix} \hat{G}^{\mathrm{R}} & \hat{G}^{\mathrm{K}} \\ 0 & \hat{G}^{\mathrm{A}} \end{pmatrix}. \tag{18}$$

If we describe superconductors, each entry of this matrix is still a 2×2 matrix in Nambu space.

The retarded and advanced Green's functions $G^{R(A)}$ determine what we will call spectral, i.e. energy-dependent properties of the system. Their Eilenberger equations have just the standard form, viz. eqn (9). Usually they can be obtained by analytical continuation of the Matsubara Green's function if we set $\omega \longrightarrow -iE \pm 0$. On the other hand, G^{K} is needed to account for properties of the system which depend on the nonequilibrium distribution function. We will later relate it to this physical quantity and indicate ways to calculate it. Expectation values of physical quantities can again be related to the Green's functions, now defined on the Keldysh contour [4–6, 35]. For instance the electrical current becomes

$$\boldsymbol{j}(\boldsymbol{r}) = -eN_0 \int_{-\infty}^{\infty} dE \,\mathrm{Tr}\langle \boldsymbol{v}_{\mathrm{F}} \hat{\tau}_3 \hat{g}^{\mathrm{K}}(\boldsymbol{v}_{\mathrm{F}}, \boldsymbol{r}, E)\rangle. \tag{19}$$

2.4. The dirty limit

2.4.1. Usadel equations in Matsubara technique

Frequently, the superconducting material has strong impurity scattering and is described by the so-called 'dirty limit'. The requirement is that the elastic scattering self-energy dominates all other terms in the Eilenberger equation. In this limit the electron motion is diffusive and the Green's functions are nearly isotropic, i.e. one can expand the Green's functions in spherical harmonics

$$\hat{g}_\omega(\boldsymbol{r}, \boldsymbol{v}_{\mathrm{F}}) = \hat{G}_\omega(\boldsymbol{r}) + \boldsymbol{v}_{\mathrm{F}} \hat{\boldsymbol{g}}_\omega(\boldsymbol{r}). \tag{20}$$

Following the prevailing convention we denote the angular average of the quasiclassical Green's function again by a capital letter. In the expansion we assumed that $\boldsymbol{v}_{\mathrm{F}} \hat{\boldsymbol{g}} \ll \hat{G}$. From the normalization condition (11), it follows that $\hat{G}_\omega^2(\boldsymbol{r}) = 1$ and $\{\hat{G}_\omega(\boldsymbol{r}), \hat{\boldsymbol{g}}_\omega(\boldsymbol{r})\} = 0$. Angular averaging of (9) yields

$$-\frac{1}{3} v_{\mathrm{F}}^2 [\hat{\boldsymbol{\partial}}_{\boldsymbol{r}}, \hat{\boldsymbol{g}}_\omega(\boldsymbol{r})] = [\omega\hat{\tau}_3 + \hat{\Delta}(\boldsymbol{r}), \hat{G}_\omega(\boldsymbol{r})], \tag{21}$$

while averaging of (9) after multiplication by $\boldsymbol{v}_{\mathrm{F}}$, yields

$$\hat{\boldsymbol{g}}_\omega(\boldsymbol{r}) = -\tau \hat{G}_\omega(\boldsymbol{r}) [\hat{\boldsymbol{\partial}}_{\boldsymbol{r}}, \hat{G}_\omega(\boldsymbol{r})]. \tag{22}$$

Here the condition $\hat{g}(\boldsymbol{r})/\tau \gg \omega\hat{\tau}_3 + \hat{\Delta}$ has been used. Inserting (22) into (21) leads to the Usadel equation [45],

$$D[\hat{\boldsymbol{\partial}}_{\boldsymbol{r}}, \hat{G}_\omega(\boldsymbol{r})[\hat{\boldsymbol{\partial}}_{\boldsymbol{r}}, \hat{G}_\omega(\boldsymbol{r})]] = [\omega\hat{\tau}_3 + \hat{\Delta}(\boldsymbol{r}), \hat{G}_\omega(\boldsymbol{r})], \tag{23}$$

where $D = v_{\mathrm{F}}^2 \tau/3$ is the diffusion constant. This equation is much simpler than the original Eilenberger equations and has been widely applied to describe properties of mesoscopic proximity systems.

The current in the dirty limit becomes

$$\boldsymbol{j}(\boldsymbol{r}) = -i \frac{\pi \sigma_{\mathrm{N}}}{2e} T \sum_\omega \mathrm{Tr}\hat{\tau}_3 \hat{G}_\omega(\boldsymbol{r}) [\hat{\boldsymbol{\partial}}_{\boldsymbol{r}}, \hat{G}_\omega(\boldsymbol{r})], \tag{24}$$

where $\sigma_{\mathrm{N}} = 2e^2 N_0 D$ is the normal-state conductivity. Note, that additional restrictions on the mean free path are necessary for this local relation to hold. We will discuss this in Section 3.2, e.g. for a bulk superconductor with a real order parameter it is given by

$$\boldsymbol{j}(\boldsymbol{r}) = -\pi \sigma_{\mathrm{N}} T \sum_\omega \frac{\Delta^2}{\Omega^2} \boldsymbol{A}(\boldsymbol{r}), \tag{25}$$

which demonstrates an important property of the dirty limit, namely a local supercurrent field relation.

2.4.2. The Usadel equation for Keldysh Green's functions

The reduction to the dirty limit can also be performed, similar to the procedure outlined above, for the Keldysh Green's functions. The Usadel equation in Keldysh $\times$ Nambu space thus reads

$$D[\hat{\boldsymbol{\partial}}_{\boldsymbol{r}}, \check{G}(E,\boldsymbol{r})[\hat{\boldsymbol{\partial}}_{\boldsymbol{r}}, \check{G}(E,\boldsymbol{r})]] = [-iE\check{\tau}_3 + \check{\Delta}, \check{G}(E,\boldsymbol{r})], \tag{26}$$

where

$$\check{\tau}_3 = \begin{pmatrix} \hat{\tau}_3 & 0 \\ 0 & \hat{\tau}_3 \end{pmatrix} \check{\Delta} = \begin{pmatrix} \hat{\Delta} & 0 \\ 0 & \hat{\Delta} \end{pmatrix}. \tag{27}$$

Although the Keldysh technique works also for time-dependent situations [4, 29], we restrict ourselves here to stationary nonequilibrium problems. Further, we only consider structures in which all superconducting reservoirs are at voltage $V = 0$, thus avoiding effects related to the nonequilibrium Josephson effect. The normalization condition still holds in the form $\check{G}\check{G} = \check{1}$. In terms of the components of (18) it implies

$$\hat{G}^R\hat{G}^{\mathrm{R}} = \hat{G}^{\mathrm{A}}\hat{G}^{\mathrm{A}} = \hat{1}, \text{ and } \hat{G}^{\mathrm{R}}\hat{G}^{\mathrm{K}} + \hat{G}^{\mathrm{K}}\hat{G}^{\mathrm{A}} = 0. \tag{28}$$

As a consequence of the second relation, G^{K} can be parameterized as

$$\hat{G}^{\mathrm{K}} = \hat{G}^{\mathrm{R}}\hat{h} - \hat{h}\hat{G}^{\mathrm{A}}. \tag{29}$$

From the Keldysh component (i.e. upper right) of the Keldysh–Usadel equation (26) we obtain a kinetic equation of motion for the distribution matrix $\hat{h}$

$$\begin{aligned} D[\nabla^2\hat{h} + (\hat{G}^{\mathrm{R}}\nabla\hat{G}^{\mathrm{R}})\nabla\hat{h} - \nabla\hat{h}(\hat{G}^{\mathrm{A}}\nabla\hat{G}^{\mathrm{A}}) - \nabla(\hat{G}^{\mathrm{R}}(\nabla\hat{h})\hat{G}^{\mathrm{A}})] \\ -(\hat{G}^{\mathrm{R}}[\hat{\Delta},\hat{h}] - [\hat{\Delta},\hat{h}]\hat{G}^{\mathrm{A}}) + iE(\hat{G}^{\mathrm{R}}[\hat{h},\hat{\tau}_3] - [\hat{h},\hat{\tau}_3]\hat{G}^{\mathrm{A}}) = 0. \end{aligned} \tag{30}$$

Here, we made use of the fact that $G^{\mathrm{R(A)}}$ satisfy the respective components of the Usadel equation. The kinetic equation has only two independent entries. Furthermore, since it is a linear equation, we can assume $\hat{h}$ to be diagonal. Returning to the definitions, we can relate it to the distribution functions for electrons and holes

$$\hat{h} = \begin{pmatrix} 1 - 2f_{el} & 0 \\ 0 & 2f_h - 1 \end{pmatrix}, \tag{31}$$

where the energy is measured from the chemical potential of the superconductor. In thermal equilibrium, for instance in the reservoirs at voltage V_R, it can be expressed by the Fermi functions

$$\hat{h}_{eq} = \begin{pmatrix} 1 - 2f(E) & 0 \\ 0 & 2f(-E) - 1 \end{pmatrix} = \begin{pmatrix} \tanh\left(\frac{E+eV_R}{2T}\right) & 0 \\ 0 & \tanh\left(\frac{E-eV_R}{2T}\right) \end{pmatrix}. \tag{32}$$

For practical calculations, it is convenient to split the distribution matrix into odd and even components with respect to the Fermi surface $\hat{h} = f_{\mathrm{L}} + f_{\mathrm{T}}\hat{\tau}_3$. The notation $f_{\mathrm{L/T}}$ refers to 'longitudinal' and 'transverse' changes of the order parameter associated with the respective nonequilibrium distributions [46, 47]. Here it is sufficient to mention that deviations of f_{L} from equilibrium are related to an effective temperature change, whereas f_{T} is related to an effective chemical potential shift. The equilibrium forms in the reservoirs are

$$f_{\mathrm{L(T)}} = \frac{1}{2}\left[\tanh\left(\frac{E+V_R}{2T}\right) + (-)\tanh\left(\frac{E-V_R}{2T}\right)\right]. \tag{33}$$

We can recover the usual electron distribution function in the end of the calculation as $2f(E) = 1 - f_{\mathrm{L}}(E) - f_{\mathrm{T}}(E)$.

The kinetic equations for the two components reduce to two coupled diffusion equations

$$\nabla(\mathcal{D}_{\mathrm{T}}\nabla f_{\mathrm{T}}) + 2\mathrm{Im}\{j_E\}\nabla f_{\mathrm{L}} = 2\frac{\mathcal{R}}{D} f_{\mathrm{T}} \tag{34}$$

$$\nabla(\mathcal{D}_{\mathrm{L}}\nabla f_{\mathrm{L}}) + 2\mathrm{Im}\{j_E\}\nabla f_{\mathrm{T}} = 0 \tag{35}$$

with energy-dependent spectral quantities

$$2\mathrm{Im}\{j_E\} = \frac{1}{4}\mathrm{Tr}[\hat{\tau}_3(\hat{G}^{\mathrm{R}}\hat{\nabla}\hat{G}^{\mathrm{R}} - \hat{G}^{\mathrm{A}}\hat{\nabla}\hat{G}^{\mathrm{A}})], \tag{36}$$

$$\mathcal{D}_{\mathrm{T}} = \frac{1}{4}\mathrm{Tr}(1 - \hat{G}^{\mathrm{R}}\hat{\tau}_3\hat{G}^{\mathrm{A}}\hat{\tau}_3), \tag{37}$$

$$\mathcal{D}_{\mathrm{L}} = \frac{1}{4}\mathrm{Tr}(1 - \hat{G}^{\mathrm{R}}\hat{G}^{\mathrm{A}}), \tag{38}$$

$$\mathcal{R} = \frac{1}{4}\mathrm{Tr}[\hat{\Delta}(\hat{G}^{\mathrm{R}} + \hat{G}^{\mathrm{A}})]. \tag{39}$$

Note, that the diffusion constant is generalized to energy-dependent spectral diffusion coefficients, $\mathcal{D}_{\mathrm{T/L}}(E)$. They are even functions of energy, whereas the the spectral supercurrent, j_E, is an odd function of the energy. Recently it has been argued, in some particular situations, that the diffusion equation should be supplemented by another term usually neglected [48].

The right-hand side of eqn (34) implies that f_{T} relaxes to 0 inside the superconductor on a scale of ξ_0, i.e. it adjusts the chemical potential to that of the superconductor. In contrast, the right-hand-side of eqn (35) vanishes. This component f_{L} relaxes only due to inelastic processes, which are neglected here, on a longer length scale [46].

2.4.3. Physical quantities and Keldysh Green's functions

We now list some results for physical quantities expressed by Keldysh–Usadel Green's functions. The self-consistency equation for the order parameter reads in analogy to (15)

$$\Delta = \frac{\lambda}{4i}\int_{-\infty}^{\infty} dE\, f_{\mathrm{L}}(F^{\mathrm{R}} - F^{\mathrm{A}}), \tag{40}$$

while the current becomes

$$j = \frac{\sigma_{\mathrm{N}}}{2}\int dE\,\mathrm{Tr}[\hat{\tau}_3(\hat{G}^{\mathrm{R}}\nabla\hat{G}^{\mathrm{K}} + \hat{G}^{\mathrm{K}}\nabla\hat{G}^{\mathrm{A}})]. \tag{41}$$

We can now use the parameterization of the Keldysh Green's function by distribution functions, eqn (29), and obtain terms proportional to the two distribution functions and their respective derivatives. By studying the parity of the terms in energy we note that some terms vanish, and we end up with the supercurrent

$$j_{\mathrm{s}} = \frac{\sigma_{\mathrm{N}}}{2}\int_{-\infty}^{\infty} dE\, f_{\mathrm{L}}(E)\mathrm{Im}\{j_E\} \tag{42}$$

and the dissipative current component

$$j_{\mathrm{n}} = \frac{\sigma_{\mathrm{N}}}{2}\int_{-\infty}^{\infty} dE\,\mathcal{D}_{\mathrm{T}}(E)\nabla f_{\mathrm{T}}(E). \tag{43}$$

The kinetic equation (34) guarantees the conservation of the total current, $j = j_s + j_n$, in the normal metal. The other kinetic equation (35) can be identified as describing the convective part of the thermal current.

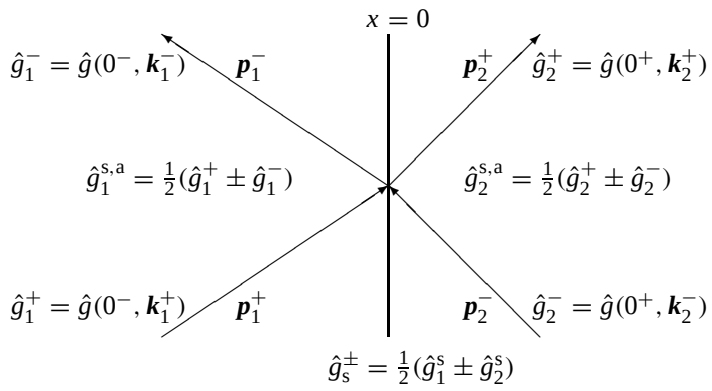

Fig. 1. Trajectories at an interface. The parallel momenta are conserved, but for different Fermi velocities on both sides the perpendicular momenta differ. The Green's functions on the trajectories involved are indicated by $\hat{g}_{1,2}^{+,-}$.

2.5. Boundary conditions

In the quasiclassical approximation, the information on length scales of the order of the Fermi wavelength have been integrated out. Consequently, one can no longer account directly for the effect of potential barriers or interfaces on this level. It turns out, however, from a study of the full theory, that potential barriers and interfaces can be accounted for by effective boundary conditions for the quasiclassical Green's functions. A derivation of boundary conditions valid at arbitrary transmission of the interface has been given by Zaitsev [49]. These boundary conditions couple the classically transmitted and reflected trajectories. The corresponding wavevectors $\boldsymbol{k}_{1,2}^{\pm}$ are shown in Fig. 1.

The in- and outgoing Green's functions $\hat{g}_{1,2}^{\pm}$ on both sides (1 and 2) of these trajectories are combined as indicated in Fig. 1. They fulfill the boundary conditions

$$\begin{aligned} \hat{g}_1^{\mathrm{a}} &= \hat{g}_2^{\mathrm{a}}, \\ \hat{g}^{\mathrm{a}}[R(\hat{g}_{\mathrm{s}}^+)^2 + (g_{\mathrm{s}}^-)^2] &= T\hat{g}_{\mathrm{s}}^-\hat{g}_{\mathrm{s}}^+, \end{aligned} \tag{44}$$

where $R = 1 - T$ is the momentum-dependent reflection coefficient. The functions $\hat{g}_{1,2}^{\mathrm{a}}$ and $\hat{g}_{\mathrm{s}}^{+,-}$ are defined in Fig. 1. Note, that current conservation through the boundary is ensured by the first of these equations. The boundary conditions are also valid for Keldysh Green's function, provided the Nambu matrices are replaced by Keldysh matrices.

The boundary conditions can be simplified in the dirty limit for low transparencies of the interfaces. As was shown by Kuprianov and Lukichev [50] they read in this limit

$$\begin{aligned} p_{F1}^2 l_1 \hat{G}_1 \frac{d}{dx}\hat{G}_1 &= p_{F2}^2 l_2 \hat{G}_2 \frac{d}{dx}\hat{G}_2, \\ l_2 \hat{G}_2 \frac{d}{dx} G_2 &= t[\hat{G}_2, \hat{G}_1]. \end{aligned} \tag{45}$$

Here $t = \langle p_{\mathrm{F}2x} T / p_{\mathrm{F}2} R \rangle$ is a (small) parameter related to the transparency, and $p_{\mathrm{F}2x}$ is the projection of the Fermi momentum onto the normal of the interface. Recently Lambert *et al*. [51] showed that the second of these conditions constitutes the first term of an expansion in the parameter t, and they calculated the second term in this expansion.

2.6. Parameterizations

For the further handling of the quasiclassical equations, both numerically and analytically, two parameterizations have turned out to be especially useful: the Riccati- and the θ-parameterization.

2.6.1. Riccati parameterization

We will make use of the Riccati parameterization mostly in equilibrium problems for general strength of the impurity scattering. In this case we write the Matsubara Green's functions as [52]

$$\hat{g}_\omega(\boldsymbol{r}, \boldsymbol{v}_\mathrm{F}) = \frac{1}{1+aa^\dagger}\begin{pmatrix} 1-aa^\dagger & 2a \\ 2a^\dagger & -1+aa^\dagger \end{pmatrix}, \tag{46}$$

where the functions $a_\omega(\boldsymbol{r}, \boldsymbol{v}_\mathrm{F})$ and $a^\dagger_\omega(\boldsymbol{r}, \boldsymbol{v}_\mathrm{F})$ obey the equations

$$\begin{aligned} -\boldsymbol{v}_\mathrm{F}\nabla a &= 2\tilde{\omega}a + \tilde{\Delta}^* a^2 - \tilde{\Delta}, \\ \boldsymbol{v}_\mathrm{F}\nabla a^\dagger &= 2\tilde{\omega}a^\dagger + \tilde{\Delta} a^{\dagger 2} - \tilde{\Delta}^*. \end{aligned} \tag{47}$$

Here

$$\tilde{\omega} = \omega + \langle g\rangle/2\tau \text{ and } \tilde{\Delta} = \Delta + \langle f\rangle/2\tau \tag{48}$$

are the renormalized energy and pair potential. These equations are of the Riccati type. The functions a and $a^\dagger$ appearing in this parameterization are directly related to the coefficients of the Andreev amplitudes. This can be seen, by noting that (47) in the clean limit directly follow from the Andreev equations [3] identifying $a = u/v$ [53]. For numerical purposes these equations are well suited, since they are two *uncoupled stable* differential equations (one for each direction of integration). This should be contrasted to the original Eilenberger equations, which are coupled and unstable differential equations. These equations also provide a basis to treat the linear response to an external field [12, 54].

2.6.2. θ parameterization

The dirty-limit equations, which do not dependent on $\boldsymbol{v}_\mathrm{F}$ anymore, allow a simpler parameterization

$$\begin{aligned} \hat{G}^\mathrm{R}(E, \boldsymbol{r}) &= \begin{pmatrix} \cosh(\theta) & \sinh(\theta)\exp(i\chi) \\ -\sinh(\theta)\exp(-i\chi) & -\cosh(\theta) \end{pmatrix} \\ \hat{G}^\mathrm{A}(E, \boldsymbol{r}) &= \begin{pmatrix} -\cosh(\bar{\theta}) & -\sinh(\bar{\theta})\exp(i\bar{\chi}) \\ \sinh(\bar{\theta})\exp(-i\bar{\chi}) & \cosh(\bar{\theta}) \end{pmatrix}. \end{aligned} \tag{49}$$

Here, $\theta(E, \boldsymbol{r})$ and $\chi(E, \boldsymbol{r})$ are complex functions the bar denotes complex conjugation.[‡]The Usadel equations in the normal metal are now written as

$$\begin{aligned} D\partial_x^2\theta &= -2iE\sinh\theta + \frac{D}{2}(\partial_x\chi)^2\sinh 2\theta \\ \partial_x j_E &= 0,\ j_E = 2\sinh^2\theta\,\partial_x\chi. \end{aligned} \tag{50}$$

In imaginary time, it is more convenient to parameterize [55]

$$\hat{g}_\omega(\boldsymbol{r}) = \begin{pmatrix} \cos(\theta) & \sin(\theta)\exp(i\chi) \\ \sin(\theta)\exp(-i\chi) & -\cos(\theta) \end{pmatrix}, \tag{51}$$

[‡]It is also possible to parameterize using sin- and cos-functions. We prefer the present convention, which requires us to choose the gauge of Δ such that for a real pair potential, $\Delta = |\Delta|$, we have $\hat{\Delta} \propto \tau_2$. Compared to our previous definition in eqn (4) we have to shift the phase of the pair potential, ϕ, by a gauge transformation of the order parameter phase by $\pi/2$.

where $\theta(\omega, \boldsymbol{r})$ and $\chi(\omega, \boldsymbol{r})$ are now real functions. At the interface to a superconducting reservoir with pair amplitude $\Delta_0 e^{i\phi_0}$ (which vanishes in normal conductors), which is connected to the probe by good metallic contacts, the boundary conditions read

$$\begin{aligned} \theta &= \theta_{\mathrm{S}} = \mathrm{Arctanh}(\Delta/E), \\ \chi &= \phi_0. \end{aligned} \tag{52}$$

For a normal reservoir, we set $\theta = 0$. In the presence of tunneling barriers, the boundary condition becomes modified. For instance, if we consider a normal layer with resistance per length $\tilde{R}_{\mathrm{N}}$ coupled via a barrier with resistance R_{t} to a superconductor, the condition on θ following from eqn (45) reads

$$r_{\mathrm{t}} \partial_x \theta = \sinh(\theta - \theta_{\mathrm{S}}). \tag{53}$$

The direction of the derivative points away from the superconductor described by θ_S, and $r_{\mathrm{t}} = R_{\mathrm{t}}/\tilde{R}_{\mathrm{N}}$ is the ratio of the resistances. For the kinetic equation, eqn (35), the boundary condition is

$$r_{\mathrm{t}} D \partial_x f_{\mathrm{T/L}} = M_{\mathrm{T/L}}(f_{T0/\mathrm{L}0} - f_{\mathrm{T/L}}), \tag{54}$$

where $f_{T0/L0}$ are the components of the reservoir distribution function (33). Using the Green's functions G_S^{R} and F_S^{R} of the superconductor we defined the spectral functions

$$M_{\mathrm{T/L}} = \mathrm{Re}(G_S^{\mathrm{R}})\mathrm{Re}(G^{\mathrm{R}}) \pm \mathrm{Im}(F_S^{\mathrm{R}})\mathrm{Im}(F^{\dagger \mathrm{R}}). \tag{55}$$

2.7. Solution strategies

In some cases we can derive approximate analytical solutions, for instance by linearizing the equation (see e.g. [56]). In general, however, we have to rely on numerical solutions. To find the solution for a given transport problem, we can proceed as follows:

(1) Start with a given $\Delta(\boldsymbol{r})$.
(2) Solve the retarded Usadel equation.
(3) Take the solutions to calculate $N(E)$, j_E, and $\mathcal{D}_{L/T}$.
(4) Solve the kinetic equations.
(5) Calculate a new $\Delta(\boldsymbol{r})$, and iterate until self-consistency is achieved.

It is worth noting that considerable simplifications arise if one is only interested in equilibrium properties. Then it is possible to determine the self-consistent problem in the Matsubara representation, which is numerically much more stable than the real-time version. (In the latter, one frequently encounters the cancelation of large terms.) Even if one is interested in transport properties it is of advantage to proceed in two steps. First, the pair potential, which does not depend on energy, is determined in the Matsubara representation. Then, after self-consistency has been achieved, one proceeds to solve the real-time/ real-energy quasiclassical equations to obtain spectral quantities and the transport properties.

3. Spectral quantities and equilibrium properties

3.1. Density of states

As a first application we study of the local density of states in spatially inhomogeneous dirty systems. Examples are a normal metal in contact with a superconductor, inhomogeneous superconductors or boundaries of superconductors with unconventional symmetry. Depending on the problem, the pair potential $\Delta(\boldsymbol{r})$ has to be determined self-consistently. As mentioned above, for the ease of the numerical procedure, this is best performed in imaginary frequencies. The next task is to solve the Usadel equation for real energies

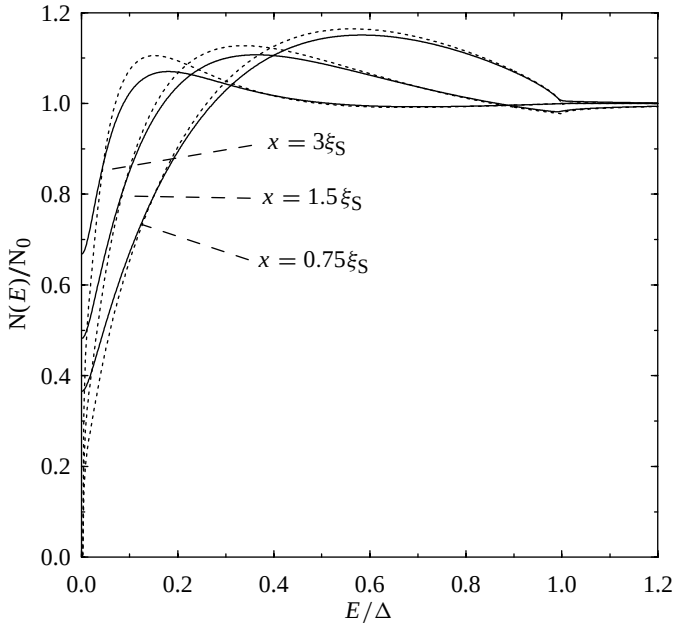

Fig. 2. Density of states on the normal side of an NS boundary for two spin-flip scattering rates: $\Gamma_{sf} = 0$ (dotted lines) and $\Gamma_{sf} = 0.015\Delta$ (solid lines).

for a given pair potential. Once we have determined the matrix Green's function $\hat{G}^{R}(E, \boldsymbol{r})$, the local density of states is given by

$$N(E, \boldsymbol{r}) = N_0 \mathrm{Re}[\hat{G}^{R}(E, \boldsymbol{r})] = N_0 \mathrm{Re}[\cosh(\theta(E, \boldsymbol{r}))], \tag{56}$$

and similar for other spectral functions.

In this chapter we will calculate the local density of states $N(E, \boldsymbol{r})$ for geometries in which a normal metal and a superconductor are in contact [8]. First, we consider the simplest case of an infinite normal metal in contact with an infinite superconductor. In this system, the spatially-resolved density of states has recently been measured with the help of tunnel junctions contacting the normal metal in different positions [9]. As a second example, we consider a finite thickness normal metal in contact with a superconductor. In this case, there is a gap in the excitation spectrum of the normal metal. The form of the density of states in this system leads to rather unusual current–voltage characteristics of SNINS tunnel junctions. This has recently been measured in proximity point contacts [57], in which the 'insulator' is an atomic point contact with variable transparency [58]. The final system examined is an overlap junction, where the normal metal and the superconductor have an finite overlap. Interestingly, in this system a local gap-like feature in the overlap region exists. In all examples in this section, the pair potential is calculated self-consistently.

3.1.1. Infinite proximity system

We consider a quasi one-dimensional geometry, i.e. an infinite normal metal is in contact with a superconductor of the same cross-section. The solution of the Usadel equations yields the DOS on the normal side at different distances from the NS boundary as shown in Fig. 2. The peak height and position change with distance. In the absence of pair-breaking effects the DOS vanishes at the Fermi level for all distances (dotted curves). Inclusion of a pair-breaking mechanism, $\Gamma_{sf} \neq 0$, (solid curves) regularizes the DOS at the Fermi level, and also suppresses the peak height. The curves are in qualitative agreement with experimental

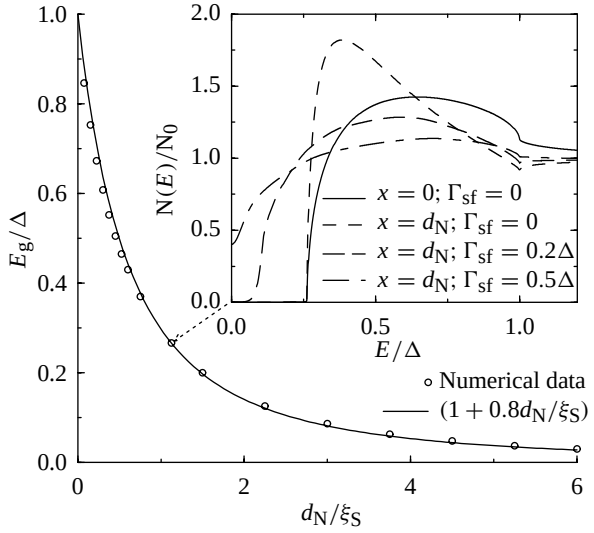

Fig. 3. Minigap E_g as a function of the normal-layer thickness. Inset: local DOS of an N-layer of thickness $d_N = 1.1\xi_S$ in proximity with a bulk superconductor.

data presented in Ref. [9]. The self-consistent calculation presented here leads to a slightly better fit than the curves derived in Ref. [9], in which a constant pair potential was assumed. In particular, the low-energy behavior of the experimental curves are reproduced better.

3.1.2. Minigap in a finite normal metal

Next we consider a normal layer with finite thickness $d_N \simeq \xi_S$ in contact with a semi-infinite superconductor occupying the half space $x < 0$. This system displays what is called a 'minigap' in the density of states of the normal metal. This gap has been first noted by McMillan [59] within a tunneling model which ignores the spatial dependence of the pair amplitude. We consider here the opposite limit, assuming perfect transparency of the interface but accounting for the spatial dependence of the Green's functions.

The boundary conditions at the interface to the superconductor remains unchanged as compared to what has been discussed above. But at the open side, $x = d_N$, the condition is $d\theta(E, x)/dx = 0$, which is the same as if the normal metal were bounded by an insulator. In this case the DOS in the normal layer develops a minigap at the Fermi energy. It is smaller than the superconducting gap, and decreases as the thickness of the normal layer is increased. Results obtained from the self-consistent treatment are shown in Fig. 3. Details of the shape of the DOS depend on the position within in the N-layer [8]. However, the magnitude of the minigap is space independent, as displayed by the inset of Fig. 3. The magnitude of the gap is expected to be related to the Thouless energy $E_{Th} \sim D/d_N^2$, which becomes a relevant energy scale in mesoscopic proximity systems. This relation has to be modified in the limit $d_N \to 0$. Indeed, as shown in Fig. 3, a relation of the form $E_g \sim (\text{const}\ \xi_S + d_N)^{-2}$ fits numerically quite well. The sum of the lengths may be interpreted as an effective thickness of the N-layer since the quasiparticle states penetrate into the superconductor to distances of the order of ξ_S. The effect of spin-flip scattering in the normal metal on the minigap structure is also shown in the inset of Fig. 3. The minigap is suppressed as Γ_{sf} is increased until it vanishes at $\Gamma_{sf} \approx 0.4\Delta$. For $\Gamma_{sf} = 0$ our results for the structure of the DOS agree with previous findings [7, 60]. A minigap was also found in heterostructures with low transparency barriers [61] and in a two-dimensional electron gas in contact to a superconductor [62]. A minigap in the DOS has also been found in a quantum dot coupled

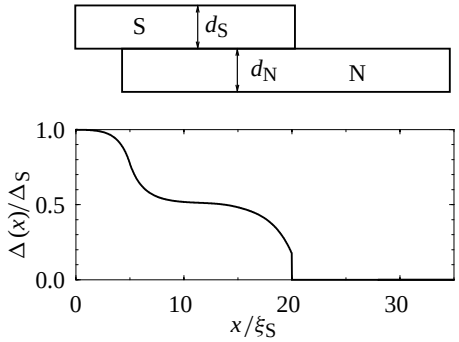

Fig. 4. Geometry and pair potential of an overlap junction for $d_S/(d_S + d_N) = 0.7$. The pair potential saturates around $0.5\Delta_S$ in the middle of the junction.

to a superconductor, if the shape of the dot is chosen such that it shows chaotic behavior in the classical limit [63]. These systems are frequently described by random matrix theory. In contrast, dot structures which are integrable in the classical limit have a nonvanishing DOS at low energy. This behavior is what one finds in a clean normal metal coupled to a superconductor [64].

3.1.3. Overlap junction

Finally, we consider a geometry in which the normal metal and the superconductor have a finite overlap region in x-direction (see Fig. 4) which is longer than ξ_S. This geometry tries to mimic the experimental realization of junctions between different metals. A measurement of the density of states along such a junction would provide additional information on the details of the proximity effect. In principle the problem is two-dimensional. But if the total thickness $d_S + d_N$ of the two layers is less than the coherence length, we can neglect all derivatives in the transverse direction and simply average the Usadel equation over the width. This result for the self-consistently determined pair potential is shown in the lower graph of Fig. 4. In the middle of the junction the pair potential saturates at $0.5\Delta_S$.

The density of states along the overlap junction develops rather interesting structures as shown in Fig. 5. The DOS evolves gradually from BCS behavior in the lowest curve, to normal metal behavior in the topmost curve. In the middle of the junction a BCS-like peak in the density of states appears at an intermediate energy due to the aforementioned plateau in the pair potential.

3.2. Magnetic response of a proximity structure

The induced superconductivity enables a normal metal to produce magnetic screening [65, 66] reminiscent of the usual Meissner effect in superconductors. However, it depends on mesoscopic scales, like the thermal coherence length $\xi_T = v_F/2\pi T$, and the thickness of the normal metal d_N [10–12, 67–74]. In addition, a length related to the penetration depth of superconductors, the London length $\lambda_N^2 \equiv 4\pi e^2 n_e/m$, plays an important role.

In the following we develop a linear response relation between the current and the vector potential, in terms of the zero-field Green's functions in the presence of arbitrary impurity concentration. We will show that this formula reproduces previous results for the magnetic screening obtained in the clean and dirty limit. Finally we show that for intermediate strength impurity scattering, qualitatively different results arise, consistent with the observations in recent experiments.

The nonlinear response of the normal metal under proximity shows interesting properties too [65, 73, 74].

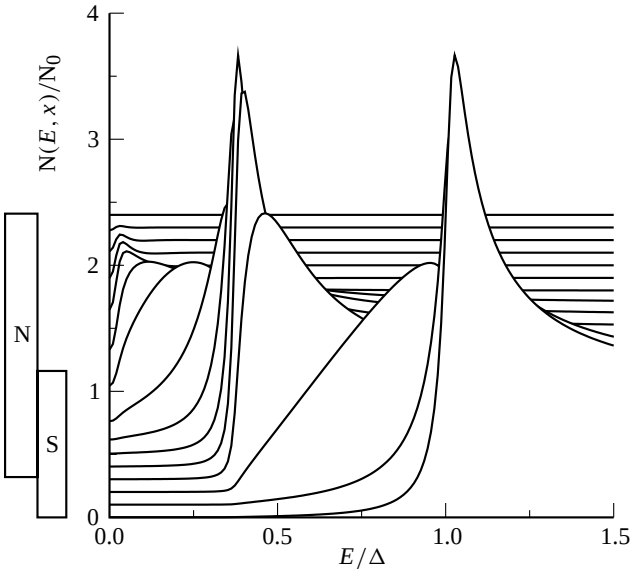

Fig. 5. Density of states along an overlap junction. The curves for different positions are offset by 0.1 on the vertical axis. The distance between two adjacent LDOS is $2.5\xi_S$ and the position is indicated by the bar on the left-hand side. One clearly sees the BCS-like density of states with reduced gap in the middle of the overlap junction.

At low temperatures, the magnetic response exhibits a first-order transition both in the clean and in the dirty limit. At a certain critical field, called the breakdown field, the induced magnetization is suddenly reduced, leading to a less diamagnetic state, or even vanishing diamagnetism in the clean case. Both the breakdown field and the size of the jump depend on temperature. All these features have been measured experimentally [10]. The qualitative agreement of the temperature dependence of the breakdown field with the clean limit theory [74] showed that the samples are close to the ballistic regime.

3.2.1. Linear response formalism

We consider the magnetic screening in linear response of a system composed of a superconductor occupying the half-space $x < 0$, in contact with a normal layer of finite thickness occupying the region $0 \leq x \leq d_N$, to a magnetic field $\boldsymbol{B}(\boldsymbol{r}) = B(x)\hat{\boldsymbol{z}}$ in the z-direction. We chose a gauge such that the vector potential is $\boldsymbol{A}(\boldsymbol{r}) = A(x)\hat{\boldsymbol{y}}$. For the analysis it is convenient to expand the Green's functions in the Riccati parameterization

$$a_\omega(v_x, v_y, x) = a^0_\omega(v_x, x) + i a^1_\omega(v_x, v_y, x) \tag{57}$$

and a similar expansion for $a^\dagger$. Here a^0 and a^1 are the first terms in an expansion in $\boldsymbol{A}$, and we have explicitly indicated the dependence on the two relevant components of $\boldsymbol{v}_F$. Accordingly, we expand the diagonal and off-diagonal Green's functions g_ω and f_ω. In first order, the Eilenberger equation reads

$$-\frac{v_x}{2}\frac{\partial}{\partial x}a^1_\omega(v_x, v_y, x) = [\tilde{\omega}(x) + \tilde{\Delta}(x)a^0_\omega(v_x, x)]a^1_\omega(v_x, v_y, x) + e v_y A(x) a^0_\omega(v_x, x). \tag{58}$$

The symmetry relation $a^1_\omega(v_x, v_y, x) = -a^1_\omega(v_x, -v_y, x)$, which is a consequence of the gauge chosen, implies that the impurity self-energies contained in $\tilde{\omega}$ and $\tilde{\Delta}$, see eqn (48), depend on a^0 only. Thus, we can integrate the linear inhomogeneous relation (58) directly. The solution still depends on the boundary conditions. Assuming perfect transparent NS boundaries and specular reflection at the boundary to the

vacuum we obtain for the current

$$j_y(x) = -\frac{e^2 p_F^2}{\pi} T \sum_{\omega>0} \int_{-\infty}^{d_N} dx' \int_0^{v_F} dv_x \frac{v_F^2 - v_x^2}{v_F^2 v_x} [1 + g_\omega^0(v_x, x)][1 - g_\omega^0(v_x, x')] \tag{59}$$
$$\times [\Theta(x - x') m_\omega(v_x, x, x') + \Theta(x' - x) m_\omega(-v_x, x, x') + m_\omega(-v_x, x, d_N) m_\omega(v_x, d_N, x')] A(x')$$
$$\equiv - \int_{-\infty}^{d_N} K(x, x') A(x') dx',$$

where $g_\omega^0(v_x, x)$ is related to $a_\omega^0(v_x, x)$ by (46), and

$$m_\omega(v_x, x, x') = \exp\left(\frac{2}{v_x} \int_x^{x'} \frac{\tilde{\Delta}(x'')}{f_\omega^{\dagger 0}(v_x, x'')} dx'' \right). \tag{60}$$

The relation (59) is characterized by the interplay between the range of the kernel determined by the decay of $m_\omega(v_x, x, x')$ and the amplitude of the prefactor $[1 + g_\omega^0(x)][1 - g_\omega^0(x')]$. This determines the nonlocality of the current–vector potential relation.

To examplify the usefulness of this result we reproduce the current response of a half-infinite superconductor. Setting $d_N = 0$, the solution of the Eilenberger equation (9) takes the simple form $g_0 = \omega/\Omega$, $f_0 = f_0^\dagger = \Delta/\Omega$, where $\Omega = (\Delta^2 + \omega^2)^{1/2}$. Inserting this in (59) we obtain the linear-response kernel

$$K_S(x, x') = \frac{e^2 p_F^2}{\pi} T \sum_{\omega>0} \frac{\Delta^2}{\Omega^2} \int_0^{v_F} du \frac{1 - u^2/v_F^2}{u} \left[e^{-(2\Omega + \frac{1}{\tau}) \frac{|x - x'|}{u}} + e^{(2\Omega + \frac{1}{\tau}) \frac{x + x'}{u}} \right]. \tag{61}$$

This result describes the current response of an arbitrary superconductor, as first derived by Gorkov [33], which here additionally includes the effect of the boundary. For fields which rapidly vary spatially we arrive at a nonlocal current-field relation of the Pippard type [75], while for slowly varying fields the kernel can be integrated out in eqn (59), producing the local London result [76].

The solution (59) is valid rather generally. We now concentrate on a structure with a normal metal of thickness d_N in contact with a semi-infinite superconductor. For simplicity we neglect the penetration of the field into the superconductor by choosing $A(x = 0) = 0$. This approximation leads to corrections to the induced magnetization of the normal metal of order λ_S/d_N only. As the second boundary condition we put $dA(x)/dx|_{x=d_N} = H$, where H is the applied magnetic field. The spatial integration is now restricted to $[0, d_N]$ and m takes the form

$$m_\omega(v_x, x, x') = \exp\left(\frac{1}{v_x \tau} \int_x^{x'} \frac{\langle f_\omega^0(x'') \rangle}{f_\omega^{\dagger 0}(v_x, x'')} dx'' \right). \tag{62}$$

Here, $\langle f_\omega^0(x) \rangle = \int_{-1}^1 du f_\omega^0(v_F u, x)$ and $f_\omega^0(v_x, x)$ is related to $a_\omega^0(v_x, x)$ by (46).

The magnetic response of the normal metal layer is expressed by the magnetic susceptibility

$$\chi = -\frac{1}{4\pi} \left[1 - \frac{A(d_N)}{H d_N} \right]. \tag{63}$$

Its calculation requires a self-consistent solution of eqn (59) and the Maxwell equation, $d^2 A(x)/dx^2 = -4\pi j_y(x)$. We will now present results for the clean and dirty limits, as well as the intermediate regime.

3.2.2. Clean limit

In the clean limit, $\tau \to \infty$, and consequently $m = 1$. Furthermore, $g^0_\omega(v_x)$ is constant in space, and the current takes the form [67]

$$j_{\text{clean}} = -\frac{1}{4\pi\lambda^2(T)d_{\text{N}}}\int_0^{d_{\text{N}}} A(x)dx, \tag{64}$$

where

$$\lambda^2(T) = \begin{cases} \lambda_{\text{N}}^2, & \text{for } T = 0, \\ \dfrac{\lambda_{\text{N}}^2 T}{12T_{\text{A}}}\exp\left(2\dfrac{T}{T_{\text{A}}}\right), & \text{for } T \gg T_{\text{A}}. \end{cases} \tag{65}$$

Here, we defined $\lambda_{\text{N}}^2 \equiv 4\pi e^2 n_{\text{e}}/m$ and the Andreev temperature $T_{\text{A}} \equiv v_{\text{F}}/(2\pi d_{\text{N}})$. The extremely nonlocal form of the current-field relation (64) leads to an overscreening for $\lambda(T) < d_{\text{N}}$. This means, the magnetic induction $B(x)$ changes its sign inside the normal metal, reaching for $\lambda_{\text{N}} \ll d_{\text{N}}$ at the interface to the superconductor a value as large as $-H/2$, which points in *opposite* direction of the external field. The characteristic temperature is given by the Andreev temperature T_{A}, which plays the same role as the Thouless energy in the diffusive case.

For the susceptibility we find

$$\chi = -\frac{1}{4\pi}\frac{3}{4 + 12\lambda^2(T)/d_{\text{N}}^2}. \tag{66}$$

In the limit $\lambda(T) \ll d_{\text{N}}$ the susceptibility is $3/4$ of $-1/4\pi$, thus, the screening is not perfectly diamagnetic. For $\lambda(T) \gg d_{\text{N}}$ screening is exponentially suppressed. Both lengths coincide, $\lambda(T) = d_{\text{N}}$, at a crossover temperature $T \sim 2T_{\text{A}}\log(d_{\text{N}}/\lambda_{\text{N}})$, which can be considerably larger than T_{A} itself. Interestingly, it is exactly this temperature below which the first-order transition in the nonlinear response occurs [74]. The result for the linear susceptibility is displayed in Fig. 6 as the thin unbroken curve.

3.2.3. Dirty limit

Next we assume that the mean free path, l, is the smallest length scale (except for the Fermi wavelength). In the absence of fields the Green's functions vary on a scale $\xi_{\text{N}} = (D/2\pi T)^{1/2}$, and the dirty-limit is realized if $l \ll \xi_{\text{N}}$. However in the situation with a space-dependent field, as seen from the kernel (59), a stronger requirement is needed. The dirty-limit form of the current-field relation (24) is found only if the vector potential changes slowly on the scale of the mean free path. Assuming this to be the case, we obtain the susceptibility shown in Fig. 6 as the thin dotted curve. The typical energy scale, below which the screening saturates is given by the Thouless energy $E_{\text{Th}} = D/d_{\text{N}}^2$ in analogy to the Andreev temperature T_{A} in the clean limit.

In order to check whether the requirement of a slowly varying vector potential is satisfied, we define a local penetration depth $\lambda(x, T)$ as

$$\frac{1}{\lambda^2(x,T)} = \frac{4\pi\tau}{\lambda_{\text{N}}^2}T\sum_{\omega>0}F_\omega^2(x). \tag{67}$$

In order to evaluate it we can proceed with the approximate form $F_\omega \sim \exp[-x(2\omega/D)^{1/2}]$. As a result we find for the local penetration depth

$$\lambda(x,T) \approx \begin{cases} \lambda_{\text{N}}x/l, & \text{if } \xi_{\text{N}}(T) \gg d_{\text{N}}, \\ \lambda_{\text{N}}\xi_{\text{N}}(T)e^{x/\xi_{\text{N}}(T)}/l, & \text{if } \xi_{\text{N}}(T) \ll d_{\text{N}}. \end{cases} \tag{68}$$

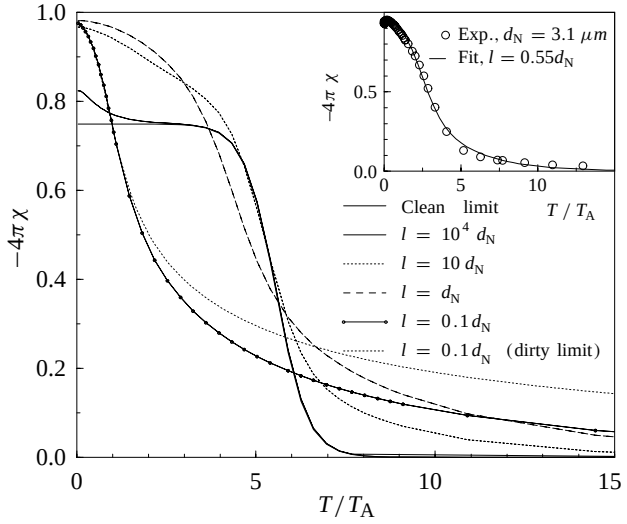

Fig. 6. The susceptibility of the normal metal layer for $\lambda_N = 0.003 d_N$. The clean limit is indicated by a thin line reaching 0.75 for $T \to 0$. Shorter mean free paths , l, (even as large as $10^4 d_N$) lead to an enhanced screening at low temperatures. For shorter mean free paths, in the diffusive regime, a completely different temperature dependence is found. The dirty limit theory including a local current response deviates strongly from the correct result at higher temperatures. Inset: comparison of experiment and theory. The thickness of the normal metal in the experiment was 3.1 μm, corresponding to $T_A = 540$ mK. The London length $\lambda_N = 22$nm was taken from the literature. To fit these samples a mean free path $l = 0.55 d_N = 1.7\ \mu$m had to be used. This is in rough agreement with the result $l = 4\ \mu$m of a transport measurement.

For the local relation to be valid we need $l < \lambda(x, T)$ in the spatial region in which the screening occurs. For $T \ll E_{Th}$ this means $l \ll \lambda(d_N)$, leading to the requirement $l^2 \ll \lambda_N d_N$. The penetration depth $\lambda(d_N)$ is then given by $\lambda_N d_N / l$. It is interesting to note that this means that full screening $\lambda(d_N) \ll d_N$ is only achieved for $l \gg \lambda_N$. For $T \gg E_{Th}$ screening takes place at $x \approx \xi_N$ and we have $l^2 \ll \lambda_N \xi_N(T)$. The low and high temperature conditions for the local approximation are different. Consequently, it is possible that the dirty-limit theory can be applied at low temperatures, whereas it fails to describe the correct behavior at higher temperatures.

A comparison of the dirty-limit result and the more general result for a fairly short mean free path $l = 0.1 d_N$, taking into account the nonlocal screening, is shown in Fig. 6. We clearly observe a difference between the two results for higher temperatures. From the above discussion it is clear that the temperature scale at which the deviation sets in is related to the Thouless energy E_{Th}, as demonstrated by the result in Fig. 6.

3.2.4. Arbitrary impurity concentration

Finally we allow for arbitrary values of the mean free path. A qualitative understanding may be gained from looking at the current vector potential relation in the limit $l \gg d_N$. In the limit $T \ll T_A$ the zeroth-order Green's functions are given by the clean limit expressions. We approximate the kernel (59) by

$$K(x, x') = \frac{1}{8\pi\lambda^2(T) d_N} [e^{-|x-x'|/l} + e^{-(2d-x-x')/l}]. \tag{69}$$

Since $l \gg d_N$, the exponentials may be expanded to first order. As a result, we obtain two contributions to the current $j(x) = j_{clean} + j_{imp}(x)$. The first contribution j_{clean} is given by the clean limit expression eqn (64).

The second is an impurity induced contribution

$$j_{\rm imp}(x) = \frac{1}{8\pi\lambda^2(T)d_{\rm N}} \int_0^{d_{\rm N}} \frac{|x-x'| + 2d_{\rm N} - x - x'}{l} A(x')dx'. \tag{70}$$

This relations demonstrates when deviations from the clean limit become important. It is clear that the impurities cannot be neglected, if $j_{\rm imp}(x)$ is comparable to $j_{\rm clean}$. We estimate this by calculating the two contributions to the current using the clean-limit vector potential. Comparing the two contributions, we find that impurities can be neglected, if

$$\lambda_{eff}^3(T) \equiv \lambda^2(T)l \gg d_{\rm N}^3. \tag{71}$$

This equation defines a new length scale, the effective penetration depth λ_{eff}. For the clean limit to be valid at $T = 0$ the condition $\lambda_{eff}(0) > d_{\rm N}$ has to be fulfilled, since in this case the screening takes place on the geometrical scale $d_{\rm N}$. In the case $\lambda_{eff}(0) \ll d_{\rm N}$ the field is screened on a scale λ_{eff} and the susceptibility is strongly enhanced in comparison to the clean limit. Nevertheless, the clean-limit behavior may reappear at higher temperatures, since $\lambda_{eff}(T)$ grows with temperature.

For $T \gg T_{\rm A}$ the deviations from the clean limit can be calculated as perturbation in the impurity scattering. The correction to g_ω^0 leads to a finite superfluid density close to the superconductor via the factor $1 - g_\omega^0(x') \approx (\xi_T/2l)\exp(-2x/\xi_T)$ in the kernel. The range of the kernel is modified by the correction to $f_\omega^{\dagger 0}$, which is nonnegligible in this case. Since $f_\omega^{\dagger 0} \approx (\xi_T/2l)\exp(-x/\xi_T)$, we find for $T \gg T_{\rm A}$

$$m_\omega(v_x, x, x') = \exp\left(\frac{1}{l}\int_x^{x'} dx'' \frac{f_\omega^0(x'')}{f_\omega^{\dagger 0}(x'')}\right) \approx \exp\left(2\frac{x'-x}{\xi_T}\right). \tag{72}$$

In deriving this equation the v_x-dependence was neglected by putting $v_x = v_{\rm F}$. The range of the kernel is now given by ξ_T, which is strongly temperature dependent. For the current we find

$$j(x) \approx \frac{1}{\lambda_{eff}^3(0)} \int_0^{d_{\rm N}} dx' e^{-2(x'+|x-x'|)/\xi_T} A(x'), \tag{73}$$

again showing the importance of the length scale λ_{eff}. In the limit $\lambda_{eff}(0) \gg \xi_T$ the field cannot be screened on the scale ξ_T, leading to a vanishing susceptibility. However, if $\lambda_{eff}(0) \ll \xi_T$ the field can be screened on a length scale smaller than ξ_T and the susceptibility will be finite.

For arbitrary mean free paths we have solved the screening problem numerically. The susceptibility as a function of temperature is shown in Fig. 6. The different curves refer to the clean limit and to mean free paths $l/d_{\rm N} = 10^4, 10, 1, 0.1$. In this plot we see the all the features discussed above. For large mean free paths the screening is enhanced in comparison with the clean limit at low and high temperatures, whereas the clean limit is restored in an intermediate temperature range. For small mean free paths ($l = 0.1d_{\rm N}$ in the graph) screening is suppressed also in the intermediate temperature range.

A comparison to experimental data from Ref. [11] is shown in the inset. Using the mean free path as the only fit parameter they can be reproduced well by the theory. Furthermore, the fitted mean free path is in rough agreement with an independent experimental estimate obtained from a resistance measurement of the same sample above the critical temperature.

3.3. Equilibrium supercurrent in a diffusive SNS junction

The supercurrent through an SNS junction had been studied in the past mostly on the level of the Ginzburg–Landau theory [77], which is valid near $T_{\rm c}$ when the order parameter is small. Recent experiments entered the mesoscopic regime at low temperatures, where, e.g. the coherence length $\xi_{\rm N} = \sqrt{D/2\pi T}$ is comparable to the sample size d. Here a more general approach is needed.

Strong deviations from the Ginzburg–Landau behavior have shown in the current through a very thin (of

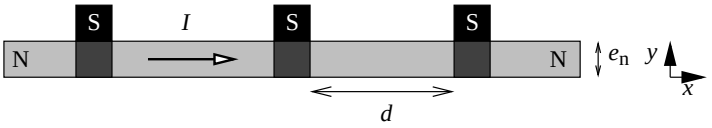

Fig. 7. A proximity wire as used in the experiment [13]. The thickness is assumed to be $e_N \ll \xi_0$ and d is the distance between the strips.

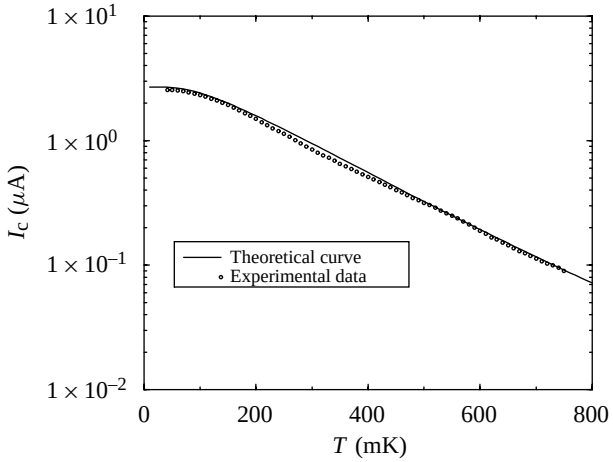

Fig. 8. Critical current of the proximity wire compared with experiment [13]: $d = 800$ nm, resistance of the N-part between two strips $R_N = 0.66\ \Omega$.

thickness e_N much smaller than ξ_0), diffusive normal wire on top of which an array of superconducting strips had been deposited [13, 22], see Fig. 7. If there is a good metallic contact between the superconductors and the wire, we can assume the Green's functions under the strips to coincide [78] with the values in the strips. These, in turn, can be assumed to be reservoirs, so the Green's functions are given by their bulk values (13). The structure is, thus, equivalent to a chain of SNS junctions without barriers between the normal metal and the superconductor.

We are interested in the equilibrium supercurrent. Hence, it is sufficient to use the Matsubara technique in the parameterization (49). We thus have to solve the Usadel equation for the Green's function with the boundary conditions (52) assuming $\phi_0 = \pm\phi/2$ at $x = \pm d/2$. The general structure of the solution is such that θ decays over a scale of $\xi_\omega = \sqrt{\mathcal{D}/2\omega}$ from the boundaries. If $\xi_\omega \ll d$, the overlap between the induced θ from the two superconductors is exponentially small. Then we can approximate the pair amplitude by a superposition of the solutions describing a semi-infinite normal part in the absence of phase gradients, i.e.

$$F_\omega(x) = e^{i\varphi/2}\sin\theta_\omega^+(x) + e^{-i\varphi/2}\sin\theta_\omega^-(x),$$
$$\tan(\theta_\omega^\pm/4) = \exp\left(\pm x\sqrt{\frac{2\omega}{D}} + A_\omega^\pm\right). \tag{74}$$

For $T \gg E_{Th} = D/d^2$ this approximate solution is sufficient to calculate the current. From the sum (14) we

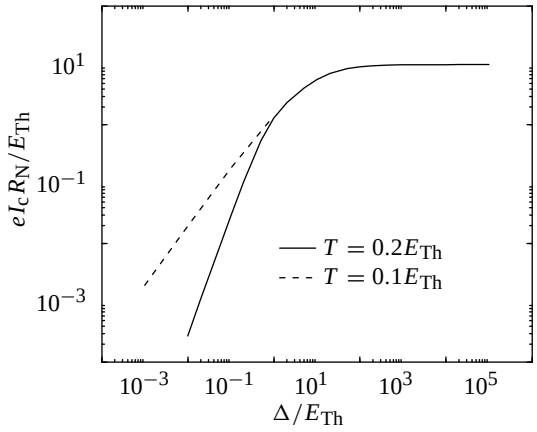

Fig. 9. The critical current at low temperature for different values of the gap, normalized to the Thouless energy. $\Delta \gg E_{\rm Th}$ corresponds to long and $\Delta \ll E_{\rm Th}$ to short junctions.

find $I = I_{\rm c} \sin\phi$, where the critical current is

$$I_{\rm c} = \frac{64\pi T}{eR_{\rm N}} \sum_{\omega} \frac{d}{\xi_\omega} \frac{\Delta^2}{[\omega + \Omega + \sqrt{2(\Omega^2 + \omega\Omega)}]^2} \exp\left(-\frac{d}{\xi_\omega}\right). \tag{75}$$

At high temperatures the sum over Matsubara frequencies is dominated by the first term. If, furthermore, $T \ll \Delta$, we arrive at [55, 79, 80]

$$I_{\rm c} = \frac{64\pi}{3 + 2\sqrt{2}} \frac{T}{eR_{\rm N}} \frac{d}{\xi_{\rm N}} \exp\left(-\frac{d}{\xi_{\rm N}}\right). \tag{76}$$

The exponent reflects the fact that the weakest part of the structure, i.e. the overlap region in the middle, defines the bottleneck for the supercurrent.

As becomes apparent, from the semi-logarithmic plot in Fig. 8, the critical current is approximately described by the numerical fit $I_{\rm c} \propto e^{-T/T^*}$, with $T^* = 12E_{\rm Th}/\pi$. This result arises because the convex exponential factor in (76), typical for diffusive metals, competes with the concave pre-exponent $T^{3/2}$. This surprising result resolves a puzzle with the interpretation of the experiments of Ref. [13]. The observed linear T-dependence of the exponent is what one would expect in a ballistic system [77, 80], whereas the experiments were performed with diffusive metals. The present result agrees well with the experimental observation [13].

At lower temperatures, all Matsubara frequencies contribute to (14) and we have to solve the Usadel equations numerically. The results are shown in Fig. 8. As $T < E_{\rm Th}$, the critical current saturates at a finite value $I_{\rm c}(T = 0)$. The numerical results at very low T (Fig. 9) indicate that for a long junction, $d \gg \xi_0$, the spatial decay of F limits the current to $I_{\rm c}R_{\rm N} \propto E_{\rm Th}$. In contrast, for a short junction the gap is the relevant cutoff and $I_{\rm c}R_{\rm N} \propto \Delta$ [81]. This agrees qualitatively with estimates derived from the low-energy expansion of the Usadel equation [79] The numerical results for the critical current under experimental conditions [13] explain the experiment quantitatively well (see Fig. 8).

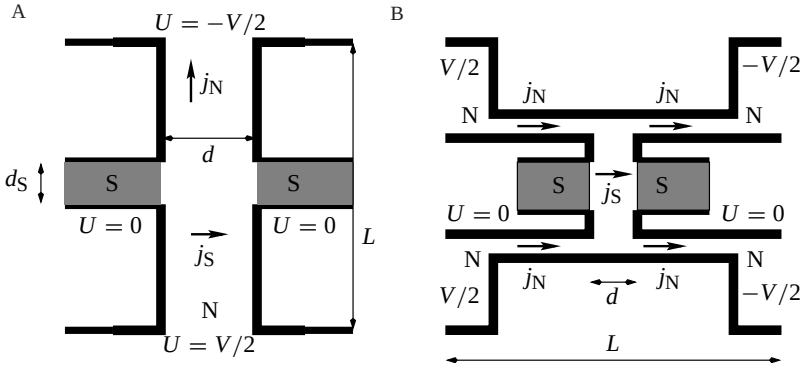

Fig. 10. Different realizations of the SNS transistors. The supercurrent is tuned by A, a perpendicular or B, a parallel normal current flow.

4. Applications to nonequilibrium transport problems

4.1. Supercurrent under nonequilibrium conditions: The SNS transistor

In this section we will describe nonequilibrium transport problems. For this purpose the Keldysh formalism outlined before is particularly appropriate. As a first example, we investigate how the supercurrent through an SNS structure is influenced by a nonequilibrium current in the normal part [15]. Specifically, we study the set-up which recently has been investigated experimentally by the Groningen group [16–18]. The device is shown in Fig. 10. Its center part is a normal conductor connecting massive reservoirs at voltages $\pm V/2$. The distribution function in this part is obtained as a solution of the kinetic equation, which for a diffusive mesoscopic normal metal reads

$$\mathcal{D}\partial_y^2 f = 0. \tag{77}$$

Its solution

$$f(E, y) = \left(\frac{1}{2} - \frac{y}{L}\right) f^{\mathrm{eq}}(E + eV/2) + \left(\frac{1}{2} + \frac{y}{L}\right) f^{\mathrm{eq}}(E - eV/2) \tag{78}$$

has two temperature-rounded steps at the electrochemical potentials of both reservoirs. The step heights depend on the position along the wire; in this way the distribution function interpolates linearly between the boundary conditions at $y = \pm L/2$. This functional dependence had been verified in the experiments of Pothier *et al*. [14]. At the center of the normal conductor, superconducting electrodes are attached, through which a supercurrent is flowing. By choosing a symmetric geometry, we can assure that the effective chemical potential of the distribution function at the site of the superconducting contacts is zero. This guarantees that no net current is flowing between the normal reservoirs and the superconducting leads. On the other hand, the nonequilibrium distribution function influences the properties of the SNS contact, and can be used to tune the supercurrent, which creates the possibility to use the device as a transistor [16]. At low temperatures even a sign reversal of the critical current, i.e. a transition to a so-called π-junction has been predicted [15] and observed [17, 18].

To describe the system we have to evaluate the spectral functions as well as the distribution function. The former can be obtained from eqn (50). The low-energy ($E \ll E_{\mathrm{Th}}$) solution, calculated perturbatively, reads

$$\begin{aligned} \theta &\simeq -i\pi/2 + (E/E_{\mathrm{Th}})a(\phi) + O(E^3) \\ \chi &\simeq \phi x/d - (E/E_{\mathrm{Th}})^2 b(\phi) + O(E^3), \end{aligned} \tag{79}$$

with real-valued functions a and b. This indicates that the spectral supercurrent $\mathrm{Im}\{j_E\}$, vanishes in this

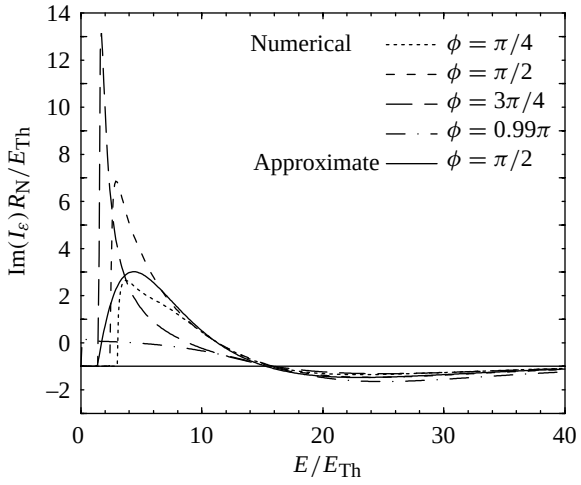

Fig. 11. The spectral current $\mathrm{Im}(j_E)$ as a function of energy for different values of the phase difference ϕ. At higher energies we find oscillations as expected from eqn (80).

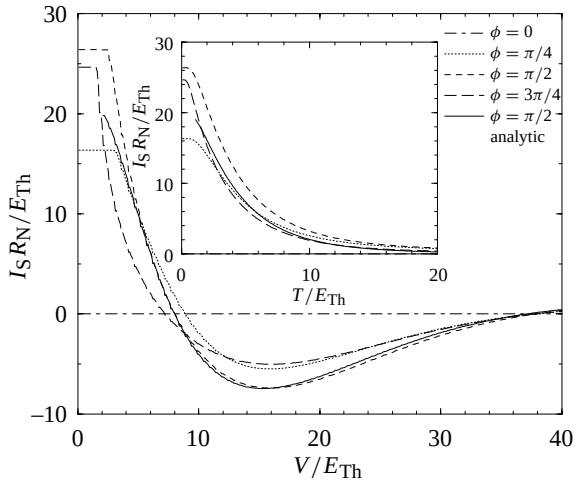

Fig. 12. The supercurrent as function of control voltage (at $T = 0$) and temperature (at $V = 0$) for various values of ϕ.

energy range. At higher energies the problem can be analyzed numerically. However, more insight into the problem is obtained from an approximate analytic solution. For the calculation of the spectral functions between the superconducting contacts we neglect the widening of the geometry in the normal metal. In this case we can use the solution (74) obtained in the previous section. The approximation introduces errors of order one in numerical coefficients, equivalent to a change in an effective area. The result for the spectral supercurrent $\mathrm{Im}\{j_E\}$, shown in Fig. 11, displays a proximity-induced minigap [8, 82] of size $E_\mathrm{g} \simeq 3.2E_\mathrm{Th}$ at $\phi = 0$. This gap decreases with increasing ϕ, when the induced pair-amplitudes from both sides start to interfere destructively, and vanishes at $\phi = \pi$ [83]. At energies directly above the gap, $\mathrm{Im}\{j_E\}$ increases sharply, but rapidly decreases at higher E. At large energies, it changes sign and eventually oscillates around zero with an exponentially decaying amplitude.

To evaluate the physical current (42), we combine the spectral supercurrent and the quasiparticle distribution function f between the reservoirs at electrochemical potentials $\pm eV/2$ derived above. Although no net current is flowing between the normal metal and the superconducting electrodes, the coupling might influence the energy dependence of the distribution. We will now show that this is not the case: compared to the distance between the reservoirs L, the proximity effect is confined to a relatively narrow region $d_{\rm S}$. For a quantitative analysis we have to distinguish between the two components $f_{\rm L/T}$, governed by the kinetic equations (34) and (35). For the supercurrent (42) we need to determine only $f_{\rm L}$. Because of the symmetry of the set-up, the component $f_{\rm T}$ vanishes at the site of the superconducting leads.

As the voltage is applied between the reservoirs, the gradients of $f_{L/T}$ point in the y-direction, i.e. perpendicular to j_E which points in the x-direction. As a consequence, the scalar products $\nabla f_{L/T} \cdot j_E$ vanish and (34) and (35) decouple. Moreover, $f_{\rm L}$ satisfies the *same* boundary conditions (33) at the two reservoirs at $\pm V/2$. Altogether, (35) implies that $f_{\rm L}$ has a constant value given by (33) throughout the wire. It is easy to check, using $2f = 1 - f_{\rm L} - f_{\rm T}$ with $f_T = 0$ and (33), that the total distribution combines to the double-step form described before.

At first glance, it may look surprising that $f_{\rm L}$ has such a strong nonequilibrium form in the normal metal next to the two superconductors, which are assumed to be in equilibrium [56]. It turns out to be a consequence of the symmetry properties of Andreev reflection. As the SN interfaces are good metallic contacts, the boundary conditions eqn (45) guarantee that at the interface $\mathcal{D}_{\rm L}$ coincides with the value in the superconductor. Thus at $|E| < \Delta$, we find from eqn (39) that $\mathcal{D}_{\rm L} = 0$. This implies that the SN interfaces decouple $f_{\rm L}$ in the normal metal from its value in the superconductor. A well known physical consequence of this property is that below the gap, when quasiparticles are transmitted by the Andreev reflection, no heat is transferred [3]. The operation of the SNS transistor without tunneling barriers is based on this very idea [16].

Our treatment of the 2D system is approximate. A more complete solution would also take the bending of supercurrent lines into account, which leads to an effective renormalization of the cross-sectional area. This problem has been solved by Volkov [56] for a related system with small d_S and tunneling barriers at the SN interface. An analysis of his solutions confirms the aforementioned argument, that the effective area of the normal region between the superconductors is larger than $d_N d$. This renormalization is reduced at higher temperature and vanishes at $T \gg E_{\rm Th}$.

The form of the distribution function implies that in the energy window, $-V/2 < E < V/2$, current-carrying states are depopulated and the supercurrent (42) is strongly suppressed. For $V < E_g$ this has no effect because of the gap. At higher voltages the supercurrent decays rapidly with increasing voltage (cf. Fig. 12). This is exactly what has been observed in the experiments [16]. Furthermore, at still larger voltages $eV \geq 10E_{\rm Th}$, the dominant contribution to the integral in (42) outside this energy window is *negative* (see Figs 11, 12), so the total supercurrent changes sign. We thus find a transition to a π-junction [84], controlled by nonequilibrium effects. This prediction has been verified in recent experiments [17, 18]. The effect is rather pronounced, the critical current of the π-junction is approximately 30% of $I_{\rm c}$ at $T = eV = 0$.

For high voltages eV or temperatures $T \gg E_{\rm g}$ we find a closed expression for the current (42). The integral is dominated by the poles of $f_{\rm L}$, given by (33), at imaginary frequencies $E = i\omega_n \pm V/2$. Also j_E can be found by analytic continuation of the approximation (74). We thus find $I_{\rm S} = I_{\rm c} \sin\phi$, with critical current

$$I_{\rm c}R_d = \frac{64\pi}{3+2\sqrt{2}} e^{-\sqrt{\Omega_V/E_{\rm Th}}} \cos\left(\frac{eV}{2\sqrt{\Omega_V E_{\rm Th}}} + \varphi_0\right) \begin{cases} eV, & \text{for } eV \gg E_{\rm g},\ T \ll E_{\rm g}, \\ T\left(\frac{(2\pi T)^2 + e^2V^2}{E_{\rm Th}^2}\right)^{\frac{1}{4}} & \text{for } T \gg E_{\rm g}. \end{cases} \tag{80}$$

Here, $\Omega_V = \pi T + \sqrt{(\pi T)^2 + (eV/2)^2}$ and

$$\varphi_0 = \begin{cases} \pi/2, & \text{for } eV \gg E_{\rm g},\ T \ll E_{\rm g}, \\ \frac{1}{2}\tan^{-1}\left(\frac{eV}{2\pi T}\right), & \text{for } T \gg E_{\rm g}. \end{cases} \tag{81}$$

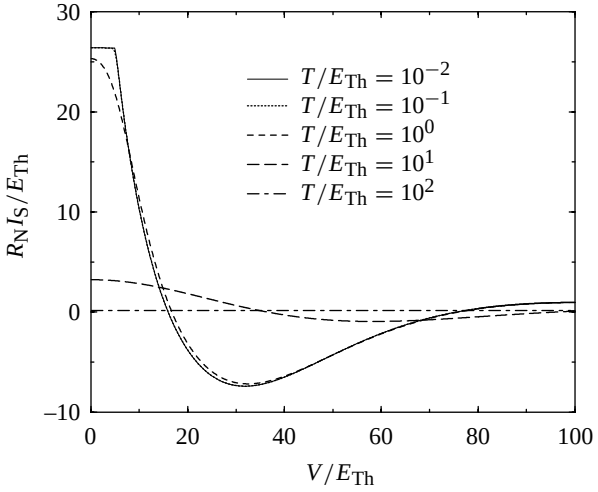

Fig. 13. The supercurrent as a function of the control voltage for various values of T at $\phi = \pi/2$.

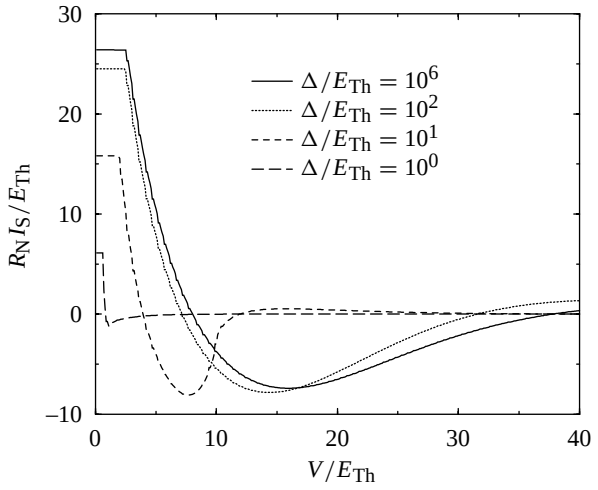

Fig. 14. The supercurrent as a function of the control voltage (at $T = 0$) for various values of Δ/E_{Th} at $\phi = \pi/2$.

This result indicates that with increasing temperature the onset of the π-junction behavior is weakened and shifted to higher voltages. Our numerical results, shown in Fig. 13, demonstrate that it is still pronounced as long as $T \leq E_{Th}$.

Above we have discussed the limit of $\Delta \gg E_{Th}$. For smaller values of Δ the minigap E_g is limited by Δ rather than E_{Th}, see Fig. 14. However, the qualitative behavior, including the transition to the π-junction regime persists.

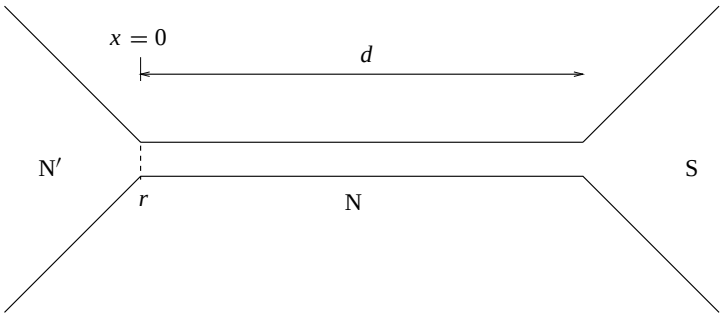

Fig. 15. A thin normal wire between normal and superconducting reservoirs.

4.2. Dissipative current in a mesoscopic wire

Perhaps the simplest system displaying the influence of the proximity effect on transport properties is shown in Fig. 15: a mesoscopic wire connects a superconducting and a normal reservoir. At the interfaces additional barriers (indicated by r in Fig. 15) may exist. In this section we assume no such barriers to be present. We assume the superconductor is assumed to be at voltage $V = 0$. As the dissipative current is a genuine nonequilibrium quantity, we will again use the Keldysh technique. In addition to the previously used boundary condition at the superconductor, we impose $\theta = 0$ at the normal reservoir. Hence, the spectral supercurrent j_E vanishes at the normal lead. As the retarded Usadel equation (50) conserves this spectral current, this implies that $j_E = 0$ everywhere and, hence, $\partial_x \chi = 0$. This means that no 'supercurrent' flows in this system. On the other hand, the 'normal' current $\boldsymbol{j}_n$ is influenced by superconducting correlations, and we have to study their behavior in an electric field.

Approximate solutions of (50) can be obtained by the same methods as described above. We will now concentrate on the case $E_{\mathrm{Th}} \ll \Delta$. For $E \ll E_{\mathrm{Th}}$, iterating (50) from the $E = 0$ solution yields

$$\theta = -\frac{8}{\pi^2}\frac{E}{E_{\mathrm{Th}}}\left[\bar{x} - \sin\left(\frac{\bar{x}\pi}{2}\right)\right] - i\frac{\pi}{2}\bar{x}, \tag{82}$$

where $\bar{x} = x/d$. For $E \gg E_{\mathrm{Th}}$ we have

$$\tanh\left(\frac{\theta}{4}\right) = -\tanh\left(\frac{i\pi}{8}\right)\exp[k(x-d)], \tag{83}$$

with $k = \sqrt{-2iE/\mathcal{D}}$. For the calculation of the dissipative current we only need the distribution function f_{T}. As $j_E = 0$, the kinetic equations decouple and (34) reduces to a simple spectral diffusion equation. Relating f_{T} to the potential and $\mathcal{D}_{\mathrm{T}}$ to the conductivity, we note that our expressions (43) and (34) are analogous to Ohm's law and the continuity equation on a spectral level, respectively. It is now straightforward to integrate (34) and to calculate the current (43), from which we obtain the differential conductance

$$G_{=} \int_{-\infty}^{\infty} \frac{dE}{2T\cosh^2[(E-V)/2T]} g(E). \tag{84}$$

Here the spectral conductance $g(E)$ is defined by

$$g(E) = G_{\mathrm{N}} d\left(\int_0^d \frac{dx}{\mathcal{D}_{\mathrm{T}}(E,x)}\right)^{-1}. \tag{85}$$

Again this expression is the spectral form of Ohm's law. Using the approximate solutions (82) and (83), we

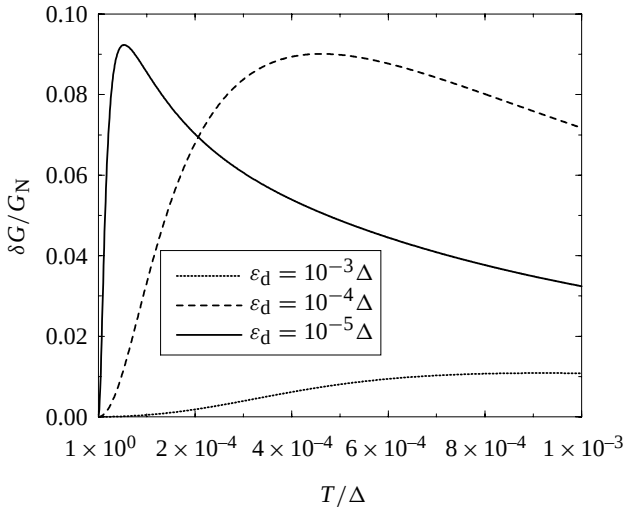

Fig. 16. Linear conductance of a proximity wire of length d with transparent interfaces. The energy is measured in units of the Thouless energy $E_{\rm Th} = D/d^2$ associated with the length d of the wire.

calculate $\mathcal{D}_{\rm T}$ and $g(E)$, and arrive, e.g. at $V = 0$, at

$$\frac{G}{G_{\rm N}} = 1 + \begin{cases} aT^2/E_d^2, & \text{for } T \ll E_{\rm Th}, \\ b\sqrt{E_{\rm Th}/T}, & \text{for } T \gg E_{\rm Th}, \end{cases} \tag{86}$$

with $a \approx 0.049$ and $b \approx 0.42$. Results are displayed in Fig. 16. The conductance approaches the normal-state value for $T \gg E_{\rm Th}$, because in this limit the proximity effect is confined to a short portion of the wire of length $\xi_{\rm N}$. However, also at $T \to 0$ the correction to the conductance vanishes. This has been first noted by Artemenko *et al.* [85] for short contacts, and later in longer wires by Nazarov and Stoof [19, 20, 86]. The theoretical prediction was confirmed in experiments [21, 22]. To the best of our knowledge, no simple physical explanation of this surprising coincidence has been provided yet. The fact that the conductance is unchanged does *not* imply that the proximity effect is absent. Even at $E = 0$ the solution (82) yields $F^{\rm R} \neq 0$, and the density of states $\mathrm{Re}(G^{\rm R})$ displays a proximity-induced gap structure, as shown in Fig. 17.

At $E = 0$, the local spectral diffusion coefficient $\mathcal{D}_{\rm T}$ coincides with the normal-state value everywhere, see eqn (82). Returning to the definition (37) and using the parameterization (49) we find here [19]

$$\mathcal{D}_{\rm T} = (\mathrm{Re}G^{\rm R})^2 + (\mathrm{Im}F^{\rm R})^2 = \cosh^2(\mathrm{Re}(\theta)) \geq 1. \tag{87}$$

This means that it is a combination of the density of states and the Maki–Thompson paraconductivity term [47, 87]. Both terms compete. At finite E, the Maki–Thompson contribution is stronger than the suppression of the DOS [19]. At $E = 0$ both contributions, although each of them varies in space, add up to 1.

In order to study the space dependence more thoroughly, we look at the local DOS in our model. Our results (17) indicate that, due to the induced superconductivity, a pseudo-gap in the DOS opens, i.e. the DOS is in general suppressed but does not vanish at low energies. If we move away from the superconductor, the pseudo-gap is weakened and the DOS approaches its normal-state form when we are close to the normal reservoir.

4.3. Supercurrent and interference effects on the dissipative current

We will extend our study of the dissipative current to a situation where also a supercurrent can flow and therefore interference of the induced correlations starts to play a role. This type of effects was first studied

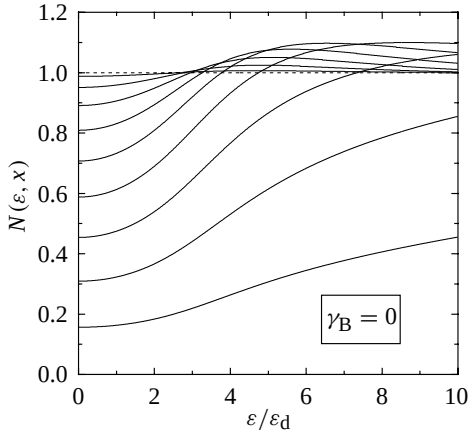

Fig. 17. Local density of states in a proximity wire with transparent interfaces for $\Delta \gg E_{Th}$ at distances $x/d = 0, 0.1, \ldots, 1.0$ (top to bottom at low E) from the normal reservoir.

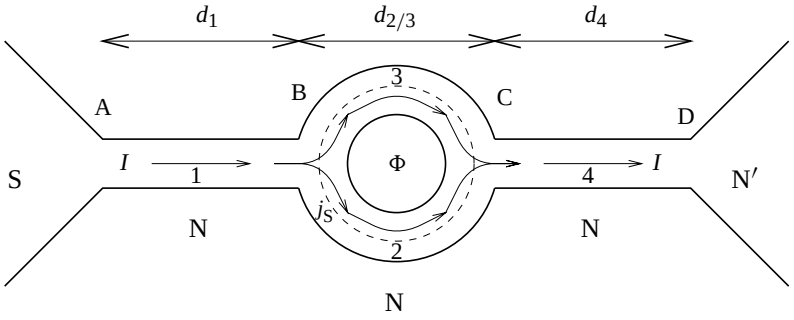

Fig. 18. A proximity wire containing a loop. The cross-sectional areas of the respective components are A_i. $\boldsymbol{j}^S$ is the field-induced supercurrent in the ring part.

experimentally [25] in cross-shaped diffusive metal structures with different superconducting leads closed by a SQUID loop, later also in analogous semiconducting structures [88], as well as in metallic structures with an Aharonov–Bohm loop [23, 89]. Usually, these structures are referred to as 'Andreev interferometers'. The common key observation is, that the conductance depends periodically on the magnetic flux penetrating the loop with a period of a superconducting flux quantum $\phi_0 = h/2e$. Moreover, it turned out that these oscillations could be detected even if $\xi_N \ll d$, where d is a typical geometrical sample dimension, i.e. the proximity effect had a longer range than expected from simpler arguments.

These effects have been extensively studied theoretically [19, 20, 31, 86, 90, 91]. We want to outline the main concepts in these systems, considering as an example the experiments of Ref. [23]. The layout of the system is shown in Fig. 18. Applying the arguments of the previous chapter, we recognize that the supercurrent is confined to the loop. Instead of dealing with the vector potential in the derivatives in (21), we remove it by a gauge transformation $\chi = \chi_0 - 2e \int_0^R dr' \boldsymbol{A}(r')$ where the integral runs around the loop. This implies that the vector potential produces an artificial phase difference of $\phi = \Phi/\Phi_0$ (modulo 2π) at one point in the loop, which we choose to be point B. This procedure already guarantees the $h/2e$ periodicity of the results.

We know from the previous sections the form of the Usadel equations in the single branches. In the present

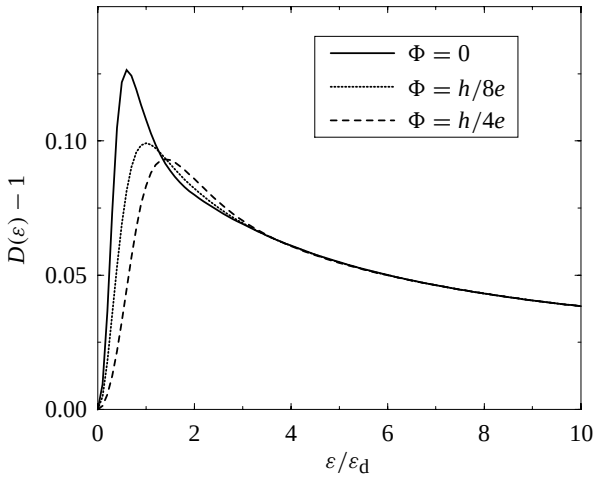

Fig. 19. Flux-dependent spectral conductance of the loop structure, assuming $A_{1/4} = 2A_{2/3}$ all $d_i = d$ and $\Delta \gg E_\mathrm{d} = D/d^2$.

problem we also have to account for the nodes. To do so we apply the idea of Zaitsev [92]: by regarding the Green's functions in the connecting wires as cross-sectional averages of the full 3D Green's function, which have well-defined derivatives in space, we will conserve the 'spectral flow'. This means

$$\check{G}_n = \check{G}_m \tag{88}$$

for all branches n and m and at nodal points we have

$$\sum_n A_n \check{G} \frac{\partial}{\partial x_n} \check{G} = 0, \tag{89}$$

where n labels the branches, and the derivatives point in the direction of branch n away from the node. This approach has been used by Nazarov [93, 94] to derive a simple circuit theory for $T = V = 0$. Here, we will assume that the branches of the loop have *half* of the cross-sectional area of the other branches.

Only very few analytical results have been derived for this system [19, 90]. Here we will focus on numerical results. As shown in Fig. 19, the spectral conductance shows a nonmonotonic shape as in the previous section. Provided that the induced correlations persist from the superconducting electrode to the loop, the low-energy results, for $E \ll E_\mathrm{Th}$, depend on the flux, whereas the conductance at $E \gg E_\mathrm{Th}$ is flux independent, see Fig. 19. This agrees with the intuition on the range of the proximity effect developed in the previous sections. In the loop, the vector potential causes the correlations to interfere destructively, so the induced conductance correction is suppressed by the presence of the loop. At $E \gg E_\mathrm{Th}$, the correlations have already decayed before they reach the loop and are therefore not influenced by the flux. On the other hand, the temperature dependent conductance also depends notably on the flux at $T > E_\mathrm{Th}$, see Fig. 20, so we indeed recover the observed long range proximity effect there [23–25]. These seemingly paradoxal observations can be resolved by examining (84). In order to calculate the conductance Fig. 20 from the spectral conductance Fig. 19, we have to convolute the latter with the derivative of the Fermi function. This distribution function is peaked around $E = 0$ and has the width T, i.e. the window of size E_Th around the Fermi surface where the spectral conductance is actually flux dependent with a relative weight of E_Th/T. Thus, the conductance depends sensitively on the contribution of this low-energy range, where the proximity effect has a long range [23], which is only limited by the phase-breaking length l_ϕ.

We note that the intuition on ξ_N, developed by regarding thermodynamic quantities as the supercurrent

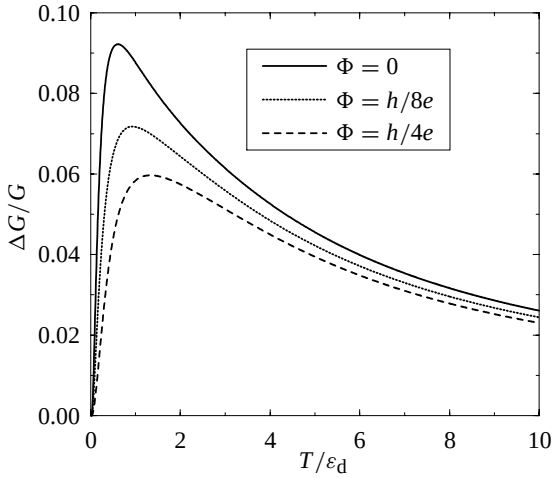

Fig. 20. Linear-response conductance of the loop as described in the caption of Fig. 19.

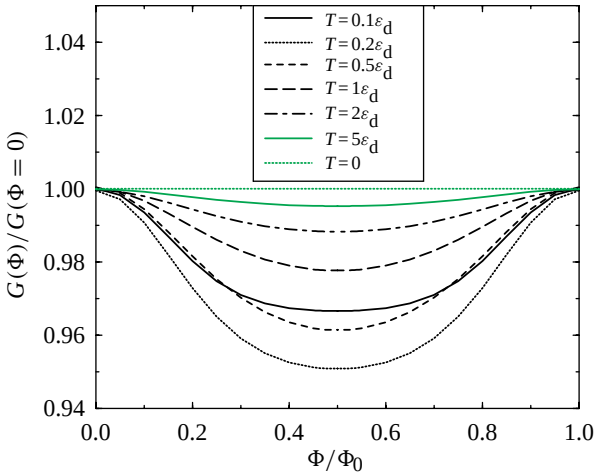

Fig. 21. Full period of normalized conductance oscillations in the loop structure at $V = 0$.

in an SNS junction (Section 3.3) fails when describing nonequilibrium quantities. On the other hand, we have shown that the same microscopic mechanism (characterized by the same Green's functions) may lead to the exponential temperature dependence of equilibrium quantities as well as to the 'long range' tail with power-law temperature dependence of nonequilibrium phenomena.

4.4. Transport through tunneling barriers

So far, we only considered situations, where the current flow does not have to overcome tunneling barriers. We found that the local spectral diffusion coefficient $\mathcal{D}_T = \cosh^2(\mathrm{Re}\theta) \geq 1$ and thereby the global conductance is always *enhanced* in comparison to the normal state. However, as we explained before (Section 3.1), the tunneling conductance is proportional to the density of states, i.e. at low energies, $E < E_{Th}$,

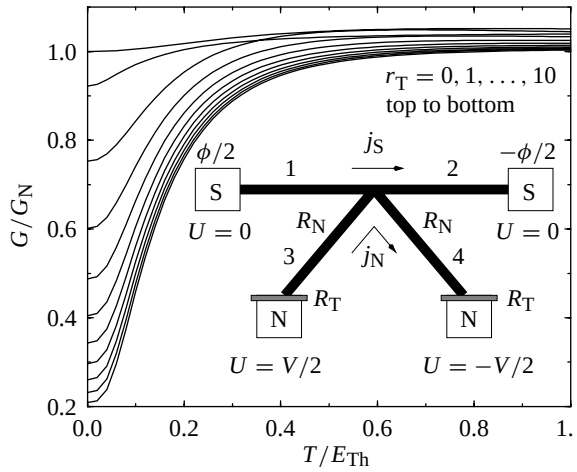

Fig. 22. Linear conductance as a function of temperature at different tunneling resistances within the diffusion/tunneling crossover at $\phi = 0$. At $\phi = \pi$ we have $G = G_N$. The inset shows the structure used for calculations. All arms 1–4 are assumed to have the same lengths d and cross sections A.

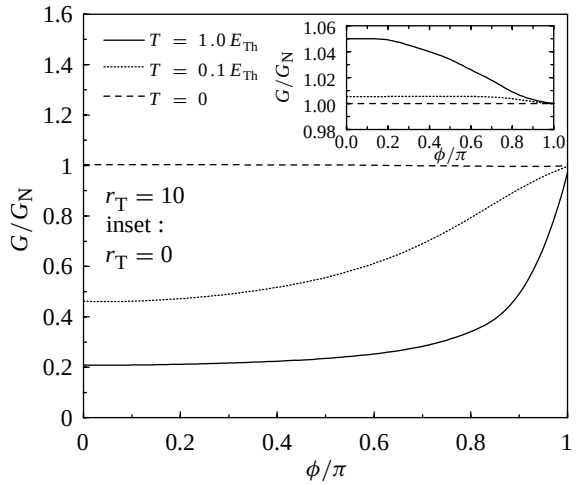

Fig. 23. Linear conductance of the interferometer in Fig. 22 as a function of the phase in the tunneling-dominated regime; inset: diffusion-dominated regime.

it is suppressed in comparison to the normal state as a manifestation of the induced superconducting gap [8, 9, 82]. In general, these two mechanisms compete. Moreover, due to the direct coupling to the normal reservoir, correlations immediately feel the presence of normal electrons and only a pseudo-gap develops, which turns into a real minigap when the reservoir is decoupled from the system via a tunneling barrier [19, 95].

Following the lines of Ref. [96] with boundary condition (54), we can calculate the distribution functions and from there the current and conductance. The result has the form (84), however, the spectral conductance now accounts for the series of the tunneling resistance and the diffusive metal

$$g(E) = G_N \frac{1 + r_T}{M(E) + r_T/\nu_T(E)}. \tag{90}$$

Here $r_T = R_T/R_N$, where R_N is the normal state resistance of the wire, and $\nu_T = \mathrm{Re}\{G^R\}$ is the reduced DOS at the interface. This result implies that already a rather low barrier of size $\sim R_N$ gives rise to a tunneling-like structure. In typical experiments, this is of order $1 \ldots 10\ \Omega$. In Figure 22, we show the conductance of a structure relevant for experiments [95] demonstrating that at low T, for $r_T > 1$, the conductance is reduced compared to the normal state value.

As we showed in Section 4.3, a magnetic flux through an Andreev interferometer causes interference effects which influence the conductance. This interference turns out to be destructive. For the system without barriers studied in Section 4.3, this manifests itself in the fact that the conductance oscillations start from a zero-flux maximum. If the interferometer contains tunneling barriers, we expect that the interference effects inside the interferometer are qualitatively not affected, however the conductance eqn (90) is dominated by tunneling into the induced gap. The destructive interference will weaken induced superconductivity and, therefore, lift the gap and consequently increase the conductance. Thus in this system we also expect magneto-conductance oscillations as described in Section 4.3, however, they will depart from a zero-flux minimum. By combining the theory of the interferometer developed in Section 4.3 with the conductance formula (90), we can study these structures and confirm this picture [95, 97]. In Figure 23, we show a half-period of the conductance oscillations at different temperatures for a tunneling-dominated system in comparison to the same system probed through metallic contacts which have a different sign of the flux dependence. This effect has also recently been observed in experiments [95].

4.5. Four-point conductance

In the previous sections we argued that the proximity effect increases the conductivity of a normal metal wire compared to the normal state. If the current is probed through tunneling barriers, this increase competes with the opening of a superconducting gap which can cause the total conductance to decrease. However, a decrease in the conductance was also observed in experiments [24, 25] where the current does not have to pass through tunneling barriers. This effect *cannot* be explained by the nonmonotonic conductance described in Section 4.2, because despite its T-dependence, the correction to the normal state conductance is still nonnegative.

In the experiments [24, 25], the current was probed by a particular four-probe configuration on a sample of appreciable width. Hence the current flow cannot be described by simple quasi-1D models as above. We will now develop a quasiclassical description of such measurements and show how the inhomogenous conductivity of the sample leads to a decrease of the four-point conductance.

Let us consider a normal film connected to a superconductor with four-point-like contacts, which lead into measuring reservoirs after a distance much larger than l_ϕ, see Fig. 24. In this configuration, the probes do not influence the spectral properties, so the solution of the retarded Usadel equation is analogous to the quasi-one dimensional case with an infinite tunneling barrier separating the normal reservoir from the sample

$$\partial_x \theta(x = d) = 0. \tag{91}$$

At large energies, θ is small and we reproduce (83). At low energies, a perturbative expansion gives

$$\theta_E(x) = \frac{E}{E_L}\frac{x}{L}\left(2 - \frac{x}{L}\right) - i\pi/2. \tag{92}$$

The kinetic equation is now two-dimensional where the current contacts are represented by source terms

$$\nabla(\mathcal{D}_T(r)\nabla f_T) = I_E(\delta(r - r_C) - \delta(r - r_D)), \tag{93}$$

A 'no current flow' condition at the normal metal edges yields

$$\partial_n f_T = 0. \tag{94}$$

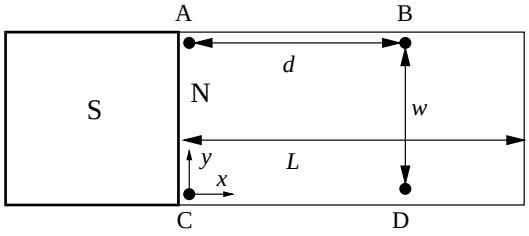

Fig. 24. A quasi-2D proximity film. The contacts A and B are used as voltage and C and D as current probes. An alternative setup: A and C are voltage probes, while the current flows through B and D.

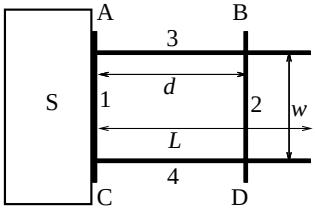

Fig. 25. A qualitatively equivalent circuit with the probe configuration as in Fig. 24.

A formal solution of eqn (34) reads

$$f_{\mathrm{T}}(E,r) = I_E(\mathcal{G}_E(r,r_C) - \mathcal{G}_E(r,r_D)), \tag{95}$$

where $\mathcal{G}_E = (\mathcal{D}_{\mathrm{T}}\nabla + \mathcal{D}_{\mathrm{T}}\nabla^2)^{-1}$ is the Green's function of the operator (34). Making use of (33), (94) and (95), and integrating I_E over energy, we obtain the total current I and arrive at the expression for the differential four-point conductance $G = dI/dV$:

$$G(V,T) = \int_0^\infty \frac{g(E)}{2T\cosh^2((E-V)/2T)}dE, \tag{96}$$

where

$$g(E) = G_{\mathrm{N}}\frac{\mathcal{G}_0^{BC} - \mathcal{G}_0^{BD} - \mathcal{G}_0^{AC} + \mathcal{G}_0^{AD}}{\mathcal{G}_E^{BC} - \mathcal{G}_E^{BD} - \mathcal{G}_E^{AC} + \mathcal{G}_E^{AD}} \tag{97}$$

is the spectral conductance. We introduced the notation $\mathcal{G}^{ij} = \mathcal{G}(r_i, r_j)$ and $\mathcal{G}_0$ is the Green's function of (34) in the normal state ($M_E(r) = \sigma_{\mathrm{N}}$). The spectral conductance (97) calculated numerically from eqns (37), (93) and (94) is presented in Fig. 26.

For narrow films the well-known results of quasi-1D calculations [19, 20] are qualitatively reproduced: the linear conductance $G(T)$ exceeds G_{N} at all temperatures, showing a nonmonotonic feature at $T \le E_d$ (for simplicity we put $L = d$ here and below). For broader films $G(T)$ *decreases* below the normal-state value at high temperatures and reaches the minimum at $T \sim 10E_{\mathrm{Th}}$. At lower T the conductance grows with decreasing T, becomes larger than G_{N} and then decreases again down to $G(T=0) = G_{\mathrm{N}}$ similarly to the 1D case (see the left inset in Fig. 26). The behavior of $g(E) \equiv G(E, T=0)$ as a function of energy (voltage) is qualitatively identical to that of $G(T)$, the negative peak at $E \sim 10E_{\mathrm{Th}}$ turns out to be even somewhat deeper.

In order to develop a semi-quantitative understanding of these results, let us consider a wire network representing the interconnections between the probes as in Fig. 25. A similar equivalent circuit model was previously used for a qualitative description of inhomogeneous superconducting films [98]. Exploiting the analogy between f_{T} and the electrical potential in a conventional circuit (see above and [26]), Kirchhoff's

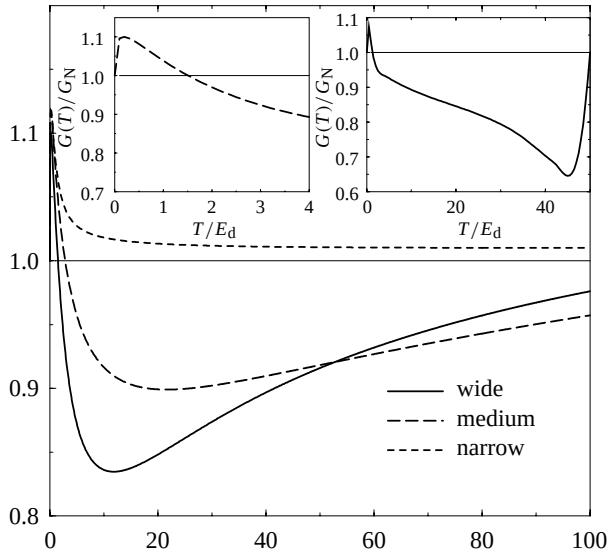

Fig. 26. The linear conductance $G(T)$ for films of different widths $w/d = 0.05, 0.5, 1.0$ calculated for $d = L$ and $T_c = 5.710^5 E_{Th}$. Left inset: the same curve at $w = 0.5d$. The T-axis is zoomed to demonstrate the presence of a usual 1D-type nonmonotonic behavior at $T \sim E_{Th}$. Right inset: $G(T)$ for a wide film and $T_c = 50E_{Th}$. The amplitude of the negative conductance peak is increased due to the effect of a superconducting gap $\Delta(T)$.

laws for the spectral conductances can be derived [19, 92]. For the present circuit Fig. 25, we find (c.f. [98])

$$g_{\text{Net}} = g_3 g_4 \sum_{i=1}^{4} g_i^{-1}, \tag{98}$$

where the g_i are the spectral conductances [19, 96] of the wires 1–4 calculated analogous to previous sections. At $T \gg E_{Th}$, only wire 1 directly attached to a superconductor acquires superconducting properties, whereas the proximity effect in the wires 2, 3 and 4 is suppressed. Thus, only g_1 increases, and $g_{2,3,4}$ remain unaffected. According to eqn (98) g_{Net} decreases below G_N. At $T \approx E_{Th}$ the proximity induced superconducting correlation penetrates into all four wires, i.e. $g_{2,3,4}$ increase, leading to the increase of g_{Net} above G_N. Close to Δ, the conductance correction has a peak corresponding to the peak in the DOS. If close to T_c, Δ becomes close to E_{Th}, the conductance of interconnection 1 is peaked and the whole effect becomes even stronger, in agreement to our numerical result.

A semi-quantitative analysis [26] shows, that the crossover energy between excess and deficit conductance is of the order of $\max(D/d^2, D/W^2)$. A careful analysis of the experiments [24, 25] shows that this explains the different signs of the conductance for different measurements [26].

5. Conclusion

We outlined the concepts of quasiclassical Green's functions. They provide a unified view of ballistic and diffusive systems in equilibrium and nonequilibrium situations. We applied the theory to describe mesoscopic proximity structures.

Acknowledgements—We acknowledge useful and stimulating discussions with V. N. Antonov, J. J. A. Baselmans, G. Blatter, H. Courtois, M. Devoret, P. Dubos, D. Estéve, A. Fauchère, M. Fogelström, A. V. Galaktionov, A. A. Golubov, S. G. den Hartog, T. M. Klapwijk, C. J. Lambert, B. Meyer, B. Müller-Allinger,

A. Morpurgo, A. C. Mota, B. Pannetier, V. Petrashov, A. Poenicke, H. Pothier, R. Raimondi, E. Scheer, R. Seviour, H. Takayanagi, A. Tagliacozzo, A. F. Volkov, H. Weber, and B. J. van Wees. This work was supported by the DFG through Sonderforschungsbereich 195 and a Graduiertenkolleg.

References

[1] G. Eilenberger, Z. Phys. **214**, 195 (1968).
[2] A. I. Larkin and Yu. N. Ovchinnikov, Zh. Eksp. Teor. Fiz. **55**, 2262 (1968) [Sov. Phys. JETP **26**, 1200 (1968)].
[3] A. F. Andreev, Zh. Eksp. Teor. Fiz. **46**, 1823 (1964) [JETP **19**, 1228 (1964)].
[4] A. Schmid, *Nonequilibrium Superconductivity*, edited by K. E. Gray (Plenum, New York, 1981).
[5] A. I. Larkin and Yu. N. Ovchinikov, *Nonequilibrium Superconductivity*, edited by D. N. Langenberg and A. I. Larkin (Elsevier, Amsterdam, 1984).
[6] J. Rammer and H. Smith, Rev. Mod. Phys. **58**, 323 (1986).
[7] A. A. Golubov and M. Yu. Kupriyanov, J. Low Temp. Phys. **70**, 83 (1988).
[8] W. Belzig, C. Bruder, and G. Schön, Phys. Rev. **B54**, 9443 (1996).
[9] S. Guéron, H. Pothier, N. O. Birge, D. Esteve, and M. Devoret, Phys. Rev. Lett. **77**, 3025 (1996).
[10] A. C. Mota, P. Visani, and A. Pollini, J. Low Temp. Phys. **76**, 465 (1989).
[11] F. B. Müller-Allinger, A. C. Mota, and W. Belzig, Phys. Rev. **B59**, 8887 (1996).
[12] W. Belzig, C. Bruder, and A. L. Fauchère, Phys. Rev. **B58**, 14531 (1998).
[13] H. Courtois, Ph. Gandit, and B. Pannetier, Phys. Rev. **B52**, 1162 (1995).
[14] H. Pothier, S. Guéron, N. O. Birge, D. Esteve, and M. H. Devoret, Phys. Rev. Lett. **79**, 3490 (1997).
[15] F. K. Wilhelm, G. Schön, and A. D. Zaikin, Phys. Rev. Lett. **81**, 1682 (1998).
[16] A. Morpurgo, B. J. van Wees, and T. M. Klapwijk, Appl. Phys. Lett. **72**, 966 (1998).
[17] J. J. A. Baselmans, A. Morpurge, B. J. van Wees, and T. M. Klapwijk, Nature **397**, 43 (1999).
[18] B. J. van Wees *et al*., Superlatt. Microstruct. **25**, (1999).
[19] A. A. Golubov, F. K. Wilhelm, and A. D. Zaikin, Phys. Rev. **B55**, 1123 (1997).
[20] Yu. V. Nazarov and T. H. Stoof, Phys. Rev. Lett. **76**, 823 (1996).
[21] P. Charlat, H. Courtois, Ph. Gandit, D. Mailly, A. F. Volkov, and P. Pannetier, Czech. J. Phys. **46**, S6 3107 (1996).
[22] H. Courtois, Ph. Gandit, B. Pannetier, and D. Mailly, Superlatt. Microstruct. **25**, 721 (1999).
[23] H. Courtois, Ph. Gandit, D. Mailly, and B. Pannetier, Phys. Rev. Lett. **76**, 130 (1996).
[24] V. T. Petrashov, V. N. Antonov, S. V. Maksimov, and R. Sh. Shaikhaidarov, Pis'ma Zh. Eksp. Teor. Fiz. **58**, 48 (1993) [JETP Lett. **58**, 49 (1993)].
[25] V. T. Petrashov, V. N. Antonov, P. Delsing, and T. Claeson, Phys. Rev. Lett. **74**, 5268 (1995).
[26] F. K. Wilhelm, A. D. Zaikin, and H. Courtois, Phys. Rev. Lett. **80**, 4289 (1998).
[27] Articles in *Mesoscopic Superconductivity*, edited by F. W. J. Hekking, G. Schön, and D. V. Averin Physica **B203**, 201 (1994).
[28] Articles in *Mesoscopic Electron Transport*, edited by L. L. Sohn, L. P. Kouwenhoven, and G. Schön (Kluwer, Dordrecht, 1997).
[29] G. Schön, *Nonequilibrium Superconductivity*, edited by D. N. Langenberg and A. I. Larkin (Elsevier, Amsterdam, 1984).
[30] C. Bruder, Supercond. Rev. **1**, 261 (1996).
[31] C. J. Lambert and R. Raimondi, J. Phys.: Condens. Matter **10**, 901 (1998).
[32] *Quasiclassical Methods in Superconductivity and Superfluidity, Proceedings of the Verditz Workshop 1996*, edited by D. Rainer and J. Sauls (1998).
[33] A. A. Abrikosov, L. P. Gorkov, and I. E. Dzyaloshinski, *Methods of Quantum Field Theory in Statistical Physics* (Dover, New York, 1963).

[34] See e.g. G. Rickayzen, *Green's Functions and Condensed Matter* (Academic Press, London, 1980); G. Mahan, *Many-Particle Physics* (Plenum, New York and London, 1981).
[35] L. P. Kadanoff and G. Baym, *Quantum Statistical Mechanics* (Benjamin, New York, 1962).
[36] Y. Nambu, Phys. Rev. **117**, 648 (1960).
[37] I. O. Kulik, Zh. Eksp. Teor. Phys. **57**, 1745 (1969) [Sov. Phys. JETP **30**, 944 (1970)].
[38] C. Ishii, Prog. Theor. Phys. **44**, 1525 (1970).
[39] U. Eckern and A. Schmid, J. Low Temp. Phys. **45**, 137 (1981).
[40] J. Eom, C. J. Chien, and V. Chandrasekhar, Phys. Rev. Lett. **81**, 437 (1998).
[41] T. Matsubara, Prog. Theor. Phys. **14**, 351 (1955).
[42] L. V. Keldysh, Zh. Eksp. Theor. Phys. **47**, 1515 (1964) [Sov. Phys. JETP **20**, 1018 (1965)].
[43] H. Smith and H. H. Jensen, *Transport Phenomena* (Clarendon, Oxford, 1989).
[44] U. Gunsenheimer and A. D. Zaikin, Phys. Rev. **B50**, 6317 (1994); Europhys. Lett. **41**, 195 (1998).
[45] K. D. Usadel, Phys. Rev. Lett. **25**, 507 (1970).
[46] A. Schmid and G. Schön, J. Low Temp. Phys. **20**, 207 (1975).
[47] M. Tinkham, *Introduction to Superconductivity* (McGraw Hill, New York, 1996) 2nd edn.
[48] A. V. Galaktionov, private communication.
[49] A. V. Zaitsev, Zh. Eksp. Teor. Fiz. **86**, 1742 (1984) [Sov. Phys. JETP **59**, 1015 (1984)].
[50] M. Yu. Kuprianov and V. F. Lukichev, Zh. Eksp. Teor. Fiz. **94**, 139 (1988) [Sov. Phys. JETP **67**, 1163 (1988)].
[51] C. J. Lambert, R. Raimondi, V. Sweeney, and A. F. Volkov, Phys. Rev. **B55**, 6015 (1997).
[52] N. Schopohl and K. Maki, Phys. Rev. **B52**, 490 (1995).
[53] N. Schopohl, in [32].
[54] M. Eschrig, PhD thesis, Universität Bayreuth, (1997) published in [32].
[55] A. D. Zaikin and G. F. Zharkov, Fiz. Nizk. Temp. **7**, 375 (1981) [Sov. J. Low Temp. Phys. (1981)].
[56] A. F. Volkov, R. Seviour, and V. V. Pavlouskii, Superlatt. Microstruct. **25**, 647 (1999).
[57] E. Scheer, private communication.
[58] E. Scheer, P. Joyez, D. Esteve, C. Urbina, and M. H. Devoret, Phys. Rev. Lett. **78**, 3535 (1997); Nature **394**, 154 (1998).
[59] W. L. McMillan, Phys. Rev. **175**, 537 (1968).
[60] A. A. Golubov, E. P. Houwman, J. G. Gijsbertsen, V. M. Krasnov, J. Flokstra, H. Rogalla, and Yu. M. Kupriyanov, Phys. Rev. **B51**, 1073 (1995).
[61] A. F. Volkov, in [27].
[62] A. F. Volkov, P. H. C. Magnée, B. J. van Wees, and T. M. Klapwijk, Physica **C242**, 261 (1995).
[63] K. M. Frahm, P. W. Brouwer, J. A. Melsen, and C. W. J. Beenakker, Phys. Rev. Lett. **76**, 2981 (1996).
[64] D. Saint-James, J. Phys. **25**, 899 (1964).
[65] Orsay Group on Superconductivity, *Quantum Fluids*, edited by D. Brewer (North-Holland, Amsterdam, 1966).
[66] Y. Oda and H. Nagano, Solid State Commun. **35**, 631 (1980).
[67] A. D. Zaikin, Solid State Commun. **41**, 533 (1982).
[68] A. C. Mota, D. Marek, and J. C. Weber, Helv. Phys. Acta **55**, 647 (1982); J. C. Weber, A. C. Mota, and D. Marek, J. Low Temp. Phys. **66**, 41 (1987).
[69] Th. Bergmann, K. H. Kuhl, B. Schröder, M. Jutzler, and F. Pobell, J. Low Temp. Phys. **66**, 209 (1987).
[70] P. Visani, A. C. Mota, and A. Pollini, Phys. Rev. Lett. **65**, 1514 (1990).
[71] A. C. Mota, P. Visani, A. Pollini, and K. Aupke, Physica **B197**, 95 (1994).
[72] S. Higashitani and K. Nagai, J. Phys. Soc. Japan **64**, 549 (1995).
[73] W. Belzig, C. Bruder, and G. Schön, Phys. Rev. **B53**, 5727 (1996).
[74] A. L. Fauchère and G. Blatter, Phys. Rev. **B56**, 14102 (1997).
[75] A. B. Pippard, Proc. R. Soc. **216**, 547 (1953).

[76] F. H. London, Proc. Phys. Soc. **A149**, 71 (1935).
[77] P. G. de Gennes, Rev. Mod. Phys. **36**, 225 (1964).
[78] M. Yu. Kupriyanov, Sov. J. Superconductivity **2**, 5 (1989).
[79] F. K. Wilhelm, A. D. Zaikin, and G. Schön, J. Low Temp. Phys. **106**, 305 (1997).
[80] A. D. Zaikin, *Nonequilibrium Superconductivity*, edited by V. L. Ginzburg (Nova Science, New York, 1988).
[81] P. Dubos *et al*., unpublished.
[82] A. A. Golubov and M. Yu. Kupriyanov, JETP **69**, 805 (1989).
[83] F. Zhou, P. Charlat, B. Spivak, and B. Pannetier, J. Low Temp. Phys. **110**, 841 (1998).
[84] L. N. Bulaevskii, V. V. Kuzii, and A. A. Sobyanin, Solid State Commun. **25**, 1053 (1977).
[85] S. N. Artemenko, A. F. Volkov, and A. V. Zaitsev, Solid State Commun. **30**, 771 (1979).
[86] T. H. Stoof and Yu. V. Nazarov, Phys. Rev. **B53**, 14496 (1996).
[87] K. Maki, Prog. Theor. Phys. **39**, 897 (1968); *ibid* **40**, 193 (1969); R. S. Thompson, Phys. Rev. **B1**, 327 (1970).
[88] S. G. den Hartog, B. J. van Wees, T. M. Klapwijk, Yu. V. Nazarov, and G. Borghs, Phys. Rev. **B56**, 13738 (1997).
[89] P. Charlat, H. Courtois, Ph. Gandit, D. Mailly, A. F. Volkov, and B. Pannetier, Phys. Rev. Lett. **77**, 4950 (1996).
[90] T. H. Stoof and Yu. V. Nazarov, Phys. Rev. **B54**, R772 (1996).
[91] A. F. Volkov, N. Allsopp, and C. J. Lambert, J. Phys.: Condens. Matter **8**, L45 (1996).
[92] A. V. Zaitsev, Physica **B203**, 274 (1994).
[93] Yu. V. Nazarov, Phys. Rev. Lett. **73**, 134 (1994).
[94] Yu. V. Nazarov, Superlatt. Microstruct. **25**, 1221 (1999).
[95] V. N. Antonov, H. Takayanagi, F. K. Wilhelm, and A. D. Zaikin, submitted to Europhys. Lett.
[96] A. F. Volkov, A. V. Zaitsev, and T. M. Klapwijk, Physica **C59**, 21 (1993).
[97] A. F. Volkov and A. V. Zaitsev, Phys. Rev. **B53**, 9267 (1996).
[98] R. Vaglio, C. Attanasio, L. Maritato, and A. Ruosi, Phys. Rev. **B47**, 15302 (1993).